



Critical review on the thermal conductivity modelling of silica aerogel composites

Ziyan Fu^a, Jorge Corker^b, Theodosios Papathanasiou^c, Yuxuan Wang^a,
Yonghui Zhou^{a,*}, Omar Abo Madyan^d, Feiyu Liao^e, Mizi Fan^{a,e,*}

^a College of Engineering, Design and Physical Sciences, Brunel University London, UB8 3PH, UK

^b IPN Led&mat, Rua Pedro Nunes, 3030 199, Coimbra, Portugal

^c Department of Civil Engineering, Aston University, B4 7ET, UK

^d SIC, Department of Engineering, University of Cambridge, Cambridge, CB2 1PZ, UK

^e College of Transportation and Civil Engineering, Fujian Agriculture and Forestry University, PR China

ARTICLE INFO

Keywords:

Aerogel composites
Modelling
Insulation
Thermal conductivity
Heat transfer

ABSTRACT

As a new generation of thermal insulation materials, the effective thermal conductivity of aerogel and its composites is extremely low. The nanoporous structure of aerogels demobilises the movement of gas molecules, and the nano-skeleton system restricts solid heat transfer because of the size effect. Numerous research and modelling works have been carried out to understand and predict heat transfers. This review thoroughly discusses the existing theories and models of silica aerogel composites in gas, solid and radiative heat transfers. It investigates the correlation of the pore size distribution and solid skeleton network of the composites with the thermal conductivity. The review then assesses the advances of the development and questions remaining for further development, including 1) some unexplainable performance of existing models and 2) improvements required for gas and solid thermal conductivity models. Bridging the identified research gaps shall lead researchers to understand existing models better, develop a more accurate model based on more realistic microstructure simulation and further innovate the models for other emerging composites.

1. Introduction

Unlike other conventional nanoporous materials, several physical properties of silica aerogel are extraordinary, such as lightweight, translucent, high specific surface area, high porosity, and extremely low thermal conductivity. Therefore, silica aerogel has broad application prospects in chemistry, heat, optics, electricity, and many other industrial applications [1,2], especially in high-efficiency thermal insulation materials for building [3–7], adsorbent materials [8–11], chemical catalysts and carriers [12–15].

The modelling work for silica aerogel composites mainly consists of three parts, namely gaseous conduction, solid conduction, and radiation, on which researchers usually focus. Although there are differences in the heat transfer of silica aerogel materials prepared by different manufacturers, based on the experiments and summary made by J. Fricke et al. [16] in 1986, we can conclude that, in aerogels, the convection of trapped gas in the pores is totally suppressed [17]. Effective thermal conductivity is calculated by summing the thermal conductivities of each way of transferring heat and the gas-solid coupling heat transfer. It is worth noting that gaseous heat

* Corresponding author. College of Engineering, Design and Physical Sciences, Brunel University London, UB8 3PH, UK.

** Corresponding author.

E-mail address: mizi.fan@brunel.ac.uk (M. Fan).

<https://doi.org/10.1016/j.job.2022.104814>

Received 15 March 2022; Received in revised form 6 June 2022; Accepted 11 June 2022

Available online 15 June 2022

2352-7102/© 2022 The Authors. Published by Elsevier Ltd. This is an open access article under the CC BY license (<http://creativecommons.org/licenses/by/4.0/>).

conduction to the effective thermal conductivity and gas thermal conductivity is different. The gaseous heat conduction to the effective thermal conductivity leads to the gas-solid coupling effect compared to the vacuumed situation. At a higher gas pressure, gaseous heat conduction to the effective thermal conductivity in a nanoporous media is even greater than that in free space [18,19]. More than half of effective thermal conductivity is contributed by gas conduction at room temperature. The mechanism of gas conductive heat transfer among aerogels has been studied since 1935. From experiment-derived empirical models [20] to analytical models [19,21–23], many researchers have taken several decades to improve the heat transfer theory of nanoporous materials, such as silica aerogel. There are two significant ways to improve the modelling of gas conduction from the base of gas kinetic theory [21], i.e. using actual pore size distribution [19,22] and considering the influence of solid skeleton on the mean free path of gas molecules [23].

Solid conduction is the second significant way of transfer in silica aerogel composites. To accurately predict the thermal conductivity of the solid phase, researchers have chosen two different routes: numerical models and analytical models. In the latest works [24–26], two ways of designing a model were considered together to some extent by many researchers. The state-of-the-art research has been trying to address the following three problems at the same time, including modelling individual nanoparticles [27], reproducing the spatial distribution of nanoparticles [26,28] and taking the additives, such as opacifiers and fibres into consideration [29].

For radiative heat transfer, theories are developed based on Rosseland diffusion theory [30]. The irregular additives can also affect the radiative heat transfer of silica aerogel composite. Mie's theory [31] has been introduced to simulate the influence of spherical additives. Lee & Cunnington's equation [32] is introduced for fibrous additives.

To date, as silica aerogel composites are more and more widely used in various sectors, especially where space and thermal insulation performance are strictly restricted, such as aerospace, military, industry and building construction, the silica aerogel composite has become a frontier hotspot in the field of materials research. Some modelling works at the level of effective thermal conductivity were made [33] most of them focused on only one aspect of heat transfer instead of considering all the ways of heat transfer organically. For silica aerogel composites, there is an existing study on the effect of fibres and opacifier on heat transfer. However, improvement can be made due to the unrealistic periodic cubic, spherical hollow model of the solid skeleton [19]. Currently, silica aerogel materials cannot be accurately predicted in terms of their thermal conductivity. The lack of this research does not match the widespread use of silica aerogels. Hence, this review investigates the models developed, examines their fitness for various materials and systems, and identifies and directs further research needs for the engineering and research community.

2. Aerogel composites as insulation materials

Aerogel has a loose foam structure with high porosity. The silica aerogel solid skeleton's particle size and pore diameter are less than 50 nm. The solid skeleton of silica aerogel includes primary and secondary particles; the dense amorphous secondary particles (1–2 nm) formed by condensation polymerisation of a silicon source are aggregated into spherical primary particles around 10 nm. A 3-D skeleton structure connects primary particles like a pearl necklace. There are a large number of pores between the nanoparticles, which makes the characteristic of low density, 100–200 kg/m³, and high porosity, 90%–99%, of the silica aerogel.

Since the pores of silica aerogel are mainly in the nanoporous range (2–50 nm), which is smaller than the free mean path of the vibration of air molecules at room temperature, around 97 nm, the heat conduction of the air in the pores is significantly inhibited [34, 35]. Therefore, silica aerogel has extremely low thermal conductivity, 12–20 mW/(m·K) at room temperature, which is much lower than conventional thermal insulation materials.

Although silica aerogel composite has perfect thermal insulation performance, the high brittleness and low strength [36] significantly limit the practical application of silica aerogel. To reduce the brittleness and increase strength, fibres are usually added to silica aerogel to enhance its mechanical properties [36–38]. In order to examine how different additives enhance the mechanical properties of aerogel composites, various additives have been tested and compared with molecular dynamics (MD) [39]. The carbon-based nanocomposites showed significantly higher toughness values in axial and lateral loadings than the native and glass fibre reinforced silica aerogel composites. Madyan et al. investigate clay aerogel composites' thermal conductivity and mechanical properties by adding Polyvinyl alcohol (PVA) of different molecular weights [40]. By only simply controlling the mixing temperature, clay-PVA aerogel's mechanical strength will be enhanced effectively; for instance, the compressive modulus will be increased by 7-folds without any increase in solid content. The hydrophilic nature of aerogel could hinder both physical and mechanical properties of aerogels by implementing environmentally friendly water-repellent agents [41], organically modifying clay aerogel composites using monomeric silicone-based chemicals and isocyanates [42], or applying an ion exchange process [43], the high moisture absorbance is addressed, as well as the physical and mechanical integrity is maintained. Furthermore, the thermal conductivity of samples including 5% clay and 5% PVA was significantly reduced by 22% from 52 to 42 W/(m·k) simultaneously to create an open-cell microstructure [44,45].

Min Cao et al. manufactured an entirely biomass-based aerogel with naturally abundant ammonium alginate (AL) and phytic acid (PA) [46]. As a result of the uniform 3-D porous structure, biomass aerogel demonstrates excellent thermal insulation performance with low thermal conductivity (34–38 mW/(m·K)). Through directional freezing and thermal imidization, an up-and-coming hydroxyapatite nanowires/polyimide (HANws/PI) composite aerogel was synthesised by the ultralong HANws combined with polyamic acid [47]. With the lowest radial thermal conductivity of 32.21 mW/(m·K) and an anisotropy factor of 2.2, the material excels at preventing additional heat loss through insulation pipes. An eco-friendly freeze-drying method followed by thermal imidization made it possible to design and synthesise this layered double hydroxide (LDH) - graphene oxide (GO) enhanced polyimide aerogel with excellent thermal insulation [48]. At room temperature, the thermal conductivity of this composite aerogel drops to 36 ± 1.7 mW/(m·K). A facile strategy was used to prepare tubular carbon aerogels from kapok fibres with improved mechanical resistance and

thermal insulation based on the tubular structures found in natural thermal insulation materials [49]. The gaseous voids in the tubular structure interfere path of heat transfer, resulting in a low thermal conductivity of 54 mW/(m·K) at 113.7 °C. All aforementioned studies above illustrate aerogel's enormous potential.

General speaking, additives such as fibre and plaster will improve the mechanical strength of aerogel composite and increase material density and thermal conductivity. A trade-off must be found to balance performance and cost of use. Nosrati et al. [50] found that 70% of aerogel-enhanced plaster had optimal balanced thermal performance and density. Another factor which influences the lifetime cost is the ageing conditions and results. From the study of Umberto et al. [51], we can conclude that the capability of aerogel-enhanced materials in maintaining their superior thermal performance can be up to 20 years. High relative humidity levels around all the ageing conditions are the most significant factors in thermal performance.

With the above processes, it is essential to note that the processes inevitably complicate the estimation of thermal conductivity of aerogel insulation materials. Aerogels are almost transparent to radiation, making pure aerogels can hardly block heat transfer with radiation. Conventionally, additives such as opacifiers are applied to decrease the effective thermal conductivity in practice [29]. In the latest research, more complicated processes are applied to break through the limits of the past. The silica aerogel composite was successfully manufactured and reinforced with a reticulated SiC skeleton (SiC/CF-Aerogel) to achieve acceptable insulation performance with thermal conductivity of 161 mW/(m·K) at 700 °C [52]. Moreover, the 3-D reinforcement enhanced the mechanical properties, including extending the performance of aerogel materials [53].

The thermal conductivity of porous materials is usually composed of the porous medium's solid and gaseous heat conduction. The solid thermal conductivity (λ_s) of materials can be expressed as [54]:

$$\lambda_s = (1 - \Pi)\lambda_{s,0} \quad (1)$$

where, Π is the porosity of the porous material and $\lambda_{s,0}$ is the intrinsic thermal conductivity of the solid. The heat conduction of the porous medium is mainly related to the porous medium, pore size distribution and pore volume. It can be seen from equation (1) that

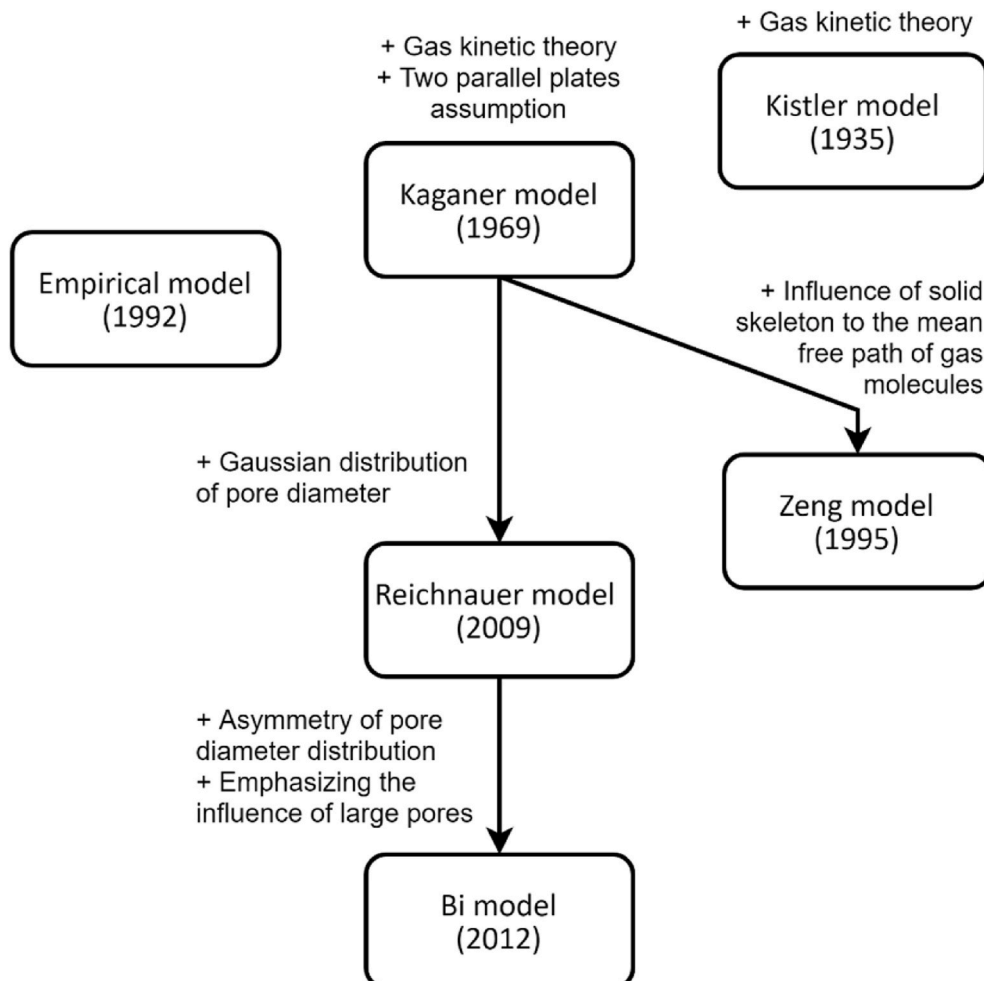


Fig. 1. Evolution of gaseous thermal conductivity in silica aerogel composites.

the lower the relative content of solids in the material, that is, the higher the porosity of the porous material, which results in the lower thermal conductivity coefficient. Silica aerogel has an ultra-high porosity of 90%–99%, so it has a low thermal conductivity and prerequisites for becoming a thermal insulation material.

3. Modelling gaseous conductive heat transfer

3.1. Evolution of models for gaseous thermal conductivity in silica aerogel composites

There are two types of gaseous thermal conductivity models in silicon aerogel composites: empirical and theoretical models. The evolution of models can be summarised in Fig. 1.

The empirical model was proposed by Fricke et al. [20] in 1992. However, the empirical model lacks necessary parameters, such as temperature and air pressure, making it valueless in reality and is no longer widely applied.

The earliest theoretical model was proposed in 1935 by Kistler et al. [55], the inventor of aerogel. Instead of hydrodynamics, Kistler used gaseous kinetic theory to explain the movement of a single gas molecule in nanoporous materials (silica aerogel) on a micro-scale and obtained the final gaseous thermal conductivity. However, as the first theoretical model, the extensive variation between the predictions and the experiments without considering the interaction between gas molecules after the pressure rises. The model also contains a coefficient that is difficult to calculate in the experiment (reflected fraction).

After more than three decades of evolution, the original Kaganer model was developed in 1969 [21]. The model has been optimised built on the previous Kistler’s model to make more accurate predictions. Unfortunately, the error between predictions and experimental results obtained by the best Kaganer-based model is still 10%.

Kaganer model introduces the Knudsen number, which is the ratio of the mean free path of the gas molecule to the pore diameter, to describe the effect of temperature and pressure on the thermal conductivity of the gas. The Kaganer model uses the two parallel plates assumption. By studying one gas molecule at a time, one can establish the relationship between the micro parameters and gaseous thermal conductivity.

Although the accuracy is not ideal, the Kaganer model is a milestone across the age. The deviation in the Kaganer model mainly results from the oversimplified consideration of the values of mean free paths of gas molecules and pore sizes of materials. The large deviation is also due to the constraint of the experiment at the time, i.e., defective experiments to determine pore sizes. To date, experiments have proven that the general concept of the Kaganer model is accurate. Almost all of the later developed models have been based on the Kaganer model.

The Kaganer model assumes that all pores in the silica aerogel have the same size, which is unrealistic. According to Reichenauer et al. aerogels can be represented by two mean pore diameters with different values; this can be expressed in the superposition form [8]. Therefore, Reichenauer et al. assumed that the pore size of the silica aerogel conformed to the Gaussian distribution and rewrote the Kaganer model accordingly. However, the normalised factor N of the Gaussian distribution is difficult to obtain and can only be calculated separately after integration.

To solve this problem, Bi et al. [23] intercepted the Gaussian distribution to only the range of $[D-3\sigma, D+3\sigma]$, thereby simplifying the calculation of the normalised factor N. Later, Bi found that the diameter of the pores of the silica aerogel was not a standard Gaussian

Table 1
Gaseous heat transfer models developed in silica aerogel.

Model	Year	Equation	Characteristics
Empirical model [20]	1992	$\lambda_g = C_g \rho^{-0.6}$	The most widely used empirical model, but the value of the gaseous thermal has nothing to do with pressure and temperature; hence, it does not match the actual situation.
Kistler model [55]	1935	$\lambda_g = 0.058a \sqrt{\frac{\bar{M}}{T}} c_v l_0 \frac{L}{2(1-a)\frac{l_0}{p} + a\left(L + \frac{l_0}{p}\right)}$	The first model which designed based on gas kinetic theory and free mean path of gaseous molecules. The size effect is considered.
Kaganer model [21]	1969	$\lambda_g = \frac{\pi \lambda_0}{1 + 2\beta Kn} = \frac{\pi \lambda_0}{1 + 2\beta \cdot l_g / D}$	The first model which designed based on two parallel plates assumption. The pore size distribution is simplified to a single value.
Reichenauer model (a.k.a. Gaussian model) [57]	2009	$\lambda_g(D, \sigma) = \frac{1}{N} \int \frac{\lambda_0}{\left(1 + \frac{2\beta l(p)}{D}\right)} e^{-\frac{1}{2} \frac{(D' - D)^2}{\sigma^2}} dD'$	It was improved from the Kaganer model, with the consideration of the Gaussian distribution of pore diameters. However, after integration, the value of factor N must be computed apart.
Bi model [23]	2012	$\lambda_g = \sum_{i=1}^n \Phi_i K(D_i)$ $\Phi_i = \begin{cases} \frac{\Delta D}{\sqrt{2\pi}\sigma} e^{-\frac{(D_i - D)^2}{2\sigma^2}} & D_i \in [D - \sigma, D + \sigma] \\ \frac{2\Delta D}{\sqrt{2\pi}\sigma} e^{-\frac{(D_i - D)^2}{2\sigma^2}} & D_i \in (D + \sigma, D + 3\sigma] \end{cases}$	Improved from Reichenauer model, with the simplified calculation and emphasised the influence of large pores. Pores with diameters outside the range $[D - \sigma, D + 3\sigma]$ are ignored, which simplifies the calculation of the normalisation factor and considers more large pores that have a significant impact on the results.
Zeng model [58]	1995	$\lambda_g = \frac{60.22 \times 10^5 p T^{-0.5} \Pi}{4.01 \times 10^9 p / T + 0.25 S_s \rho / \Pi}$	By recalculating the restricted mean free path of gas molecules, Zeng et al. improved the Kaganer model by considering the influence of the solid skeleton of nanoporous materials (silica aerogel) on the mean free path gaseous molecules.

*For the details of parameters, please refer to the next sections.

distribution. Instead, the asymmetric distribution lets the large pores have a wider distribution range than the tiny pores. In addition, the effect of large pores on the thermal conductivity of the gas is more pronounced than that of small pores. Therefore, Bi decided to consider only the pores with diameters in the range of $[D - \sigma, D + 3\sigma]$, and double the influence coefficient to the gaseous thermal conductivity of pores with diameter in $[D + \sigma, D + 3\sigma]$. This improvement made the Bi model one of the most accurate models.

However, Bi's modification of the Kaganer model is only based on qualitative analysis. Whether ignoring the influence of pores with diameters in $[D - 3\sigma, D - \sigma]$ or double the influence of pores with diameters in $[D + \sigma, D + 3\sigma]$, the extent and selection of these thresholds lack rigorous theoretical and experimental supports. This over-simplification may cause the deviation by using the Bi model, and it is also a key point worthy of further analysis and improvement by researchers.

When considering the movement of gas molecules in nanopores, the Kaganer model does not consider the influence of the solid skeleton on the mean free path of gas molecules. Based on this, Zeng et al. [56] further optimised the Kaganer model by proposing an improved mean free path calculation and obtained another accurate model.

Model development with equations of Gaseous heat transfer in silica aerogel can be summarised in Table 1, which also summarises the main characteristic of various gaseous heat transfer models.

3.2. Empirical model

The gaseous thermal conductivity value can be obtained from the experiment by comparing the total thermal conductivities before and after evacuation. If the total conductivities before and after evacuation are denoted as λ and λ_{evac} respectively, the difference $\lambda - \lambda_{evac}$ equals the gaseous conductivity λ_g . As aforementioned, the gaseous thermal conductivity could be related to pore geometry and solid substance of materials; based on this, Fricke et al. [20] has experimented with four different aerogel densities, namely $\rho = 75, 120, 150$ and 230 kg/m^3 at $T \approx 300 \text{ K}$ and predicted the gaseous thermal conductivity with their density. The experimental results are plotted in Fig. 2.

Such the experimentally derived dependences can be approximated as:

$$\lambda_g \propto \rho^\delta, \text{ with } \delta \approx -0.6 \quad (2)$$

It is worthy to note that only the gas in open-pored materials, such as aerogel, could be evacuated when the environment depressurises. In a closed-cell material, the air pressure within the pores is essentially unchanged during decompression because the gas cannot leave the closed pores. Consequently, this idea of designing comparative experiments is only valid for materials with open pores.

The logarithm of λ_s and λ_g shows their linear correlation with the logarithm of density (Fig. 3). Since the average diameter of pores decreases when ρ increases, as anticipated, λ_g reduces with growing ρ . The empirical relationship between the gas thermal conductivity of aerogel λ_g and the density ρ was further examined by introducing an empirical constant C_g . Rearranging equation (2) leads to,

$$\lambda_g = C_g \rho^{-0.6} \quad (3)$$

When the material density is $\rho = 70 \text{ kg/m}^3$, the gas thermal conductivity measured by the experiment was $\lambda_g = 0.01 \text{ W} \cdot \text{m}^{-1} \cdot \text{K}^{-1}$ [59], therefore, the empirical constant C_g , can be calculated by equation (3) as $C_g = 0.128 \text{ m}^5 \cdot \text{s}^{-3}$.

The drawbacks of this empirical model are significant. Firstly, there is little theoretical basis; the credibility of the equation is entirely dependent on experimental accuracy. Secondly, the only parameter is density ρ , which cannot fully reflect microstructure, such as the structure of the solid skeleton and the distribution of pore sizes. Thirdly, the relationship between gas thermal conductivity and pressure, temperature and humidity cannot be revealed, making it impossible to calculate high-temperature and low-pressure scenarios, such as vacuum insulated panels.

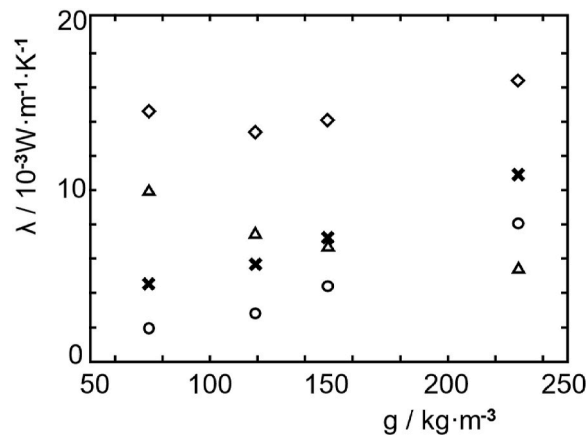


Fig. 2. ♦: Thermal conductivity of aerogel at 1 atm, ×: Thermal conductivity of aerogel at the vacuumed environment, Δ: Gaseous thermal conductivity, ○: Solid thermal conductivity (Replotted by Z. Fu) [20].

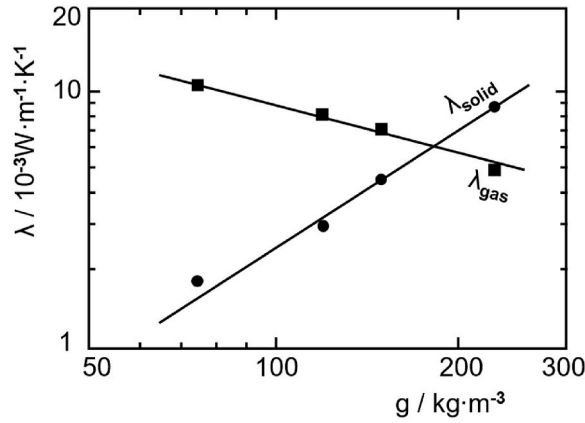


Fig. 3. Y-axis: $\log \lambda_s$ and $\log \lambda_g$, X-axis: $\log \rho$, logarithm of aerogel density. The slope for the solid is $\alpha \approx 1.5$ and slope for the gas is $\delta \approx -0.6$ (Replotted by Z. Fu) [20].

3.3. Kistler model

Hydrodynamics at the macroscopic scale investigates fluid flow in a much more extensive range than the mean free path of gaseous molecules. With hydrodynamics, regardless of the individual behaviour of molecules, the fluid is regarded as a continuous medium. However, the pore sizes of silica aerogel are at the nanoscale, smaller than the mean free path of gaseous molecules. Since the fluid flow of gas within the aerogel is a microscale fluid flow, hydrodynamics cannot be applied directly. Therefore, the Kinetic theory of gas is considered more appropriate for understanding gas flow at the microscale, as it is based on the material's microstructure to explain thermal phenomena. In 1932, Kistler et al. [55] developed the gaseous thermal conductivity model for aerogel material. The model was correlated with the molecular mean free path of gas molecules as follows:

$$\lambda_g = B c_v \eta \quad (4)$$

and

$$\eta = 0.35 \rho v l \quad (5)$$

B , in $\text{m}^2 \cdot \text{kg}^{-1}$, is a constant, c_v , in $\text{J} \cdot \text{K}^{-1} \cdot \text{m}^{-3}$, is the specific heat of the gas at constant volume, η , in $\text{kg} \cdot \text{m}^{-1} \cdot \text{s}^{-1}$, is the viscosity, ρ is the density, v is the arithmetical average velocity of the molecules, and l is the mean free path of gaseous molecules.

The gaseous thermal conductivity was finally deduced as:

$$\lambda_g = 0.058 \sqrt{\frac{M}{T}} c_v l_0 \frac{L}{L + \frac{l_0}{p}} \quad (6)$$

This equation assumes that molecules reach thermal equilibrium with the surface with each impact before leaving. M is the weight of gaseous molecular, T is the given temperature. Within an aerogel, L signifies the mean free path of a highly attenuated gas, l_0 is the typical mean free path of the gas at T and a pressure of 1 atm. Noteworthy is the fact that, due to the nanoporous structure of silica aerogel, L is usually substituted by the average pore diameter.

When only the fraction a of the molecules comes to thermal equilibrium and the fraction $1 - a$ is specularly reflected, equation (6) is rewritten as:

$$\lambda_g = 0.058 a \sqrt{\frac{M}{T}} c_v l_0 \frac{L}{2(1-a) \frac{l_0}{p} + a \left(L + \frac{l_0}{p} \right)} \quad (7)$$

Kistler, the inventor of aerogels in 1931, was the first to study how gaseous heat transfer works within the aerogel. This Kistler's model was also the first theoretical model designed to address the above problem. This model is rudimentary, and one of the drawbacks is the derivation of the coefficient 0.058. Earlier, the assumption has been made that all impacts experienced by gas molecules within aerogels occur on the surface. The assumption is very close to the truth, especially at lower pressures, but the coefficient should increase slightly at higher pressures, with more direct interactions between molecules. With higher pressure, the value of L should increase slightly, and it is no longer accurate enough to be substituted by the average pore diameter. Furthermore, neither measuring nor calculating of the reflected fraction $(1 - a)$ is easy. Therefore, for simplifying calculations, previous researchers usually assumed that $a = 1$.

3.4. Kaganer model

Aerogels are nanoporous materials typically have pores smaller than the mean free path of air (69 nm) in free space at 1 atm and

room temperature. The porous framework in a porous medium thus suppresses the motion of gas molecules; as compared to free space, gas thermal conductivity is much lower in nanopores. Kaganer described the impact of pore diameter on gaseous heat conduction using the mean free path of gas molecules and can help reveal how temperature and pressure influence gas phase thermal conductivity. As a widely used model of the gaseous thermal conductivity in micro or nanoporous media, the Kaganer model [21] was established by the assumption of two parallel plates:

$$\lambda_g = \frac{\pi\lambda_0}{1 + 2\beta Kn} \quad (8)$$

where, π is the porosity, λ_0 , in $W \cdot m^{-1} \cdot K^{-1}$, is the thermal conductivity of the gas in free space, β is a coefficient (a dimensionless constant) related to the gas accommodation and adiabatic coefficient, the coefficient β for air is 1.55, which can be calculated by equation (13) and equation (14) in the next section.

λ_0 represent the gaseous thermal conductivity in free space as follow:

$$\lambda_0^0 = (2.25\gamma - 1.25) \cdot 0.461 (p/k_B T) \cdot (8k_B T / \pi m_g)^{1/2} \cdot l_g (C_{V,g} / N_A) \quad (9)$$

where, γ is the adiabatic ratio of the gas, $k_B = 1.38 \times 10^{-23} J/K$ is Boltzmann constant, m_g is the mass of gas molecules, $C_{V,g}$, in $J \cdot K^{-1} \cdot mol^{-1}$, is mole specific heat, N_A , in mol^{-1} , is Avogadro constant.

The Knudsen number, Kn , indicates the proportion of the fluid molecules' mean free path l to the scale of representative physical length L . In this case, it is also the proportion of the mean free path of the gas molecules l_g to the average pore sizes D of the porous materials:

$$Kn = \frac{l}{L} = \frac{l_g}{D} \quad (10)$$

l_g can be computed by the following formula:

$$l_g = \frac{1}{\sqrt{2}\pi d_g^2 n_g} = \frac{1}{\sqrt{2}\pi d_g^2} \cdot \frac{1}{\frac{p}{k_B T}} = \frac{k_B T}{\sqrt{2}\pi d_g^2 p} = \frac{k_B T}{\sqrt{2}\sigma_0 p} \quad (11)$$

where, n_g , in m^{-3} , is the molecule number density of the gas, d_g is the diameter of a gas molecule, and a value of $d_g = 0.353$ nm for air molecules was taken. $\sigma_0 = \pi d_g^2$ is the cross-section of the gas molecule.

Then, one can substitute equations (10) and (11) into (8) and get

$$\begin{aligned} \lambda_g &= \frac{\pi\lambda_0}{1 + 2\beta Kn} = \frac{\pi\lambda_0}{1 + 2\beta \cdot l_g/D} = \frac{\pi\lambda_0}{1 + 2\beta \frac{k_B T}{\sqrt{2}\pi d_g^2 p} \cdot \frac{1}{\frac{k_B T}{k_B T}} \cdot \frac{l_g}{D}} = \frac{\pi\lambda_0}{1 + 2\beta \frac{k_B T}{\sqrt{2}\sigma_0 p} \cdot \frac{1}{l_g} \cdot \frac{l_g}{D}} \\ &= \frac{\pi\lambda_0}{1 + \sqrt{2}\beta \frac{k_B T}{\sigma_0 p} \cdot \frac{1}{D}} = \frac{\pi\lambda_0}{1 + \frac{\sqrt{2}\beta k_B T}{\sigma_0 D p}} \end{aligned} \quad (12)$$

Coefficient β [21] can be calculated as

$$\beta = \frac{2\gamma}{\gamma + 1} \cdot \frac{2 - \alpha}{\alpha} \cdot \frac{1}{Pr} \quad (13)$$

where, γ is the ratio of the specific heats at constant pressure and constant volume, Pr is the Prandtl number, which is defined as the ratio of momentum diffusivity to thermal diffusivity, and the correlation coefficient α (a dimensionless constant) [60] is calculated as

$$\alpha = \frac{4m_g m_s}{(m_g + m_s)^2} \quad (14)$$

where, m_g and m_s represent the weights of gas and solid molecules, respectively.

It can be found that when the mean free path of gas molecules is equivalent to the pore diameter of the system, the thermal conductivity of the gas phase will decrease significantly.

Kaganer model is one of the most popular models for gaseous thermal conductivity; it works with both analytical methods [23] and numerical methods [61] of solid heat transfer.

However, there are three possible drawbacks of the Kaganer model. Firstly, the mean free path l_g can be different in nanoporous than in the free space. Secondly, the pore diameter D of the porous media does not consider the influence of pore diameter distribution. Pore diameter distributions are frequently complex and cannot be adequately modelled by Gaussian distributions. Thirdly, some coefficients may be challenging to measure in the experimental environment.

3.5. Reichenauer model

Using the average pore diameter to describe pore distribution, the Kaganer model can analyse porous media with a very concentrated distribution of pore diameters. For more complex cases with wide pore size distribution and multiple typical pore sizes, Reichenauer et al. [19] proposed the concept of bimodal gaseous thermal conductivity for porous materials. In the case of two different pore diameters D_1 and D_2 and their respective contributions to porosity (φ_1 and φ_2), according to the model of the parallel plates, the overall gaseous thermal conductivity λ_g can be written as a linear superposition of the following two terms:

$$\lambda_g = \frac{\Pi\lambda_0\varphi_1}{1 + 2\beta l_g/D_1} + \frac{\Pi\lambda_0\varphi_2}{1 + 2\beta l_g/D_2} \tag{15}$$

By introducing the Gaussian distribution function for pore diameter distribution, Reichenauer et al. [19] enabled the calculation of the gaseous thermal conductivity of aerogel by summing the thermal conductivity of each pore:

$$\lambda_g(D, \sigma) = \frac{1}{N} \int \frac{\lambda_0}{\left(1 + \frac{2\beta l(p)}{D}\right)} e^{-\frac{1}{2}\frac{(D'-D)^2}{\sigma^2}} dD' \tag{16}$$

where, D' is the convolution variable, σ is the standard error of the Gaussian distribution of pore diameters, or the standard deviation and N is a factor that normalises the integral to provide the correct total porosity. Ideally, the value of N is the quantity of pores that should be counted. However, a model such as this one is complex and inconvenient in calculations since N cannot be calculated within the integration.

3.6. Bi model

To address the above problem from the Reichenauer model and get an approximate solution, Bi et al. [23] proposed an approximation:

$$\lambda_g = \sum_{i=1}^n \Phi_i K(D_i) \tag{17}$$

where, n is the quantity of pores, i is the index of each pore, $K(D_i)$ is the gaseous thermal conductivity of each pore (determined by pore size D_i), and Φ_i is the contribution of the pores with a diameter D_i to the overall porosity. Assuming the pores are normally distributed:

$$\Phi_i = \int_{D_i}^{D_i+\Delta D} \frac{1}{\sqrt{2\pi}\sigma} e^{-\frac{(D'-D)^2}{2\sigma^2}} dD' \approx \frac{\Delta D}{\sqrt{2\pi}\sigma} e^{-\frac{(D_i-D)^2}{2\sigma^2}} \quad (D_i > 0) \tag{18}$$

Φ_i is the probability when the pore a diameter D' locates in the diameter range of $[D_i, D_i + \Delta D]$. If only pores with a diameter within the range of $[D - 3\sigma, D + 3\sigma]$ are being considered, about 99.74% of the population of pores will be included:

$$\lim_{n \rightarrow \infty} \sum_{i=1}^n \Phi_i = \int_{D-3\sigma}^{D+3\sigma} \frac{1}{\sqrt{2\pi}\sigma} e^{-\frac{(D'-D)^2}{2\sigma^2}} dD' \approx 0.9974 \quad (D - 3\sigma > 0) \tag{19}$$

For range $[D - 3\sigma, D + 3\sigma]$, 99.74% of porous media pores are considered in calculating the λ_g . Thus, equations (18) and (19) with a computing deviation under 0.26% can be considered to be an approximate solution of equation (17).

However, according to the experiment, pore diameter distribution in the nanoporous media is not a standard Gauss distribution;

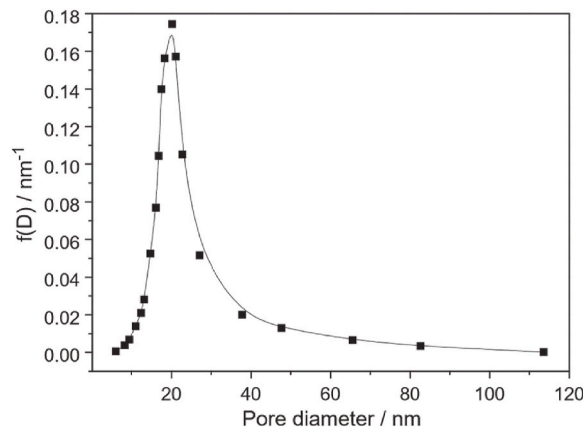


Fig. 4. Pore sizes distribution of one silica aerogel sample (Replotted by Z. Fu [23]).

large pores have a more comprehensive distribution range concerning the mean pore diameter than tiny pores, as shown in Fig. 4.

Despite the non-uniformity and asymmetry of pore diameter distributions in aerogels, the following improvement was made addressed this situation. The pore diameter distribution function assumes the following form in order to emphasise the contribution of large pores to the total thermal conductivity of gaseous systems while simultaneously decreasing the contribution of tiny pores:

$$\Phi_i = \begin{cases} \frac{\Delta D}{\sqrt{2\pi}\sigma} e^{-\frac{(D_i-D)^2}{2\sigma^2}} & D_i \in [D - \sigma, D + \sigma] \\ \frac{2\Delta D}{\sqrt{2\pi}\sigma} e^{-\frac{(D_i-D)^2}{2\sigma^2}} & D_i \in (D + \sigma, D + 3\sigma] \end{cases} \quad (20)$$

It is apparent that this model neglects the contributions from the tiny pores, which have a diameter $D_i \in [D - 3\sigma, D + \sigma)$ to the λ_g and doubles the effect from the large pores, which have a diameter $D_i \in (D + \sigma, D + 3\sigma)$.

In the previous study, the weight of the influence of a specific pore diameter on the gaseous thermal conductivity is only reflected in the number (possibility) of pores. However, this model doubles the weight of the pore in the range of $(D + \sigma, D + 3\sigma)$, emphasising the influence of large pores. The weight of the pore in the range of $[D - 3\sigma, D - \sigma]$ is set to 0; that is, their minor influence is ignored. Reichenauer et al. [19] addressed the non-uniformity problem by treating the pore diameter as a Gaussian distribution, and this model considered asymmetry through the above operations.

3.7. Zeng model

As aforementioned, one of the potential drawbacks of the Kaganer Model is that as the gas molecules in the aerogel collide, they also collide with the solid particles that lie within the aerogel. Zeng et al. assumes that the nanoscale solid skeleton changes the cross-sectional scattering area, which affects the mean free path of gas molecules. By adding a term in the denominator (lg) to represent the effect of the solid skeleton to mean free path of gas molecules, l_g becomes:

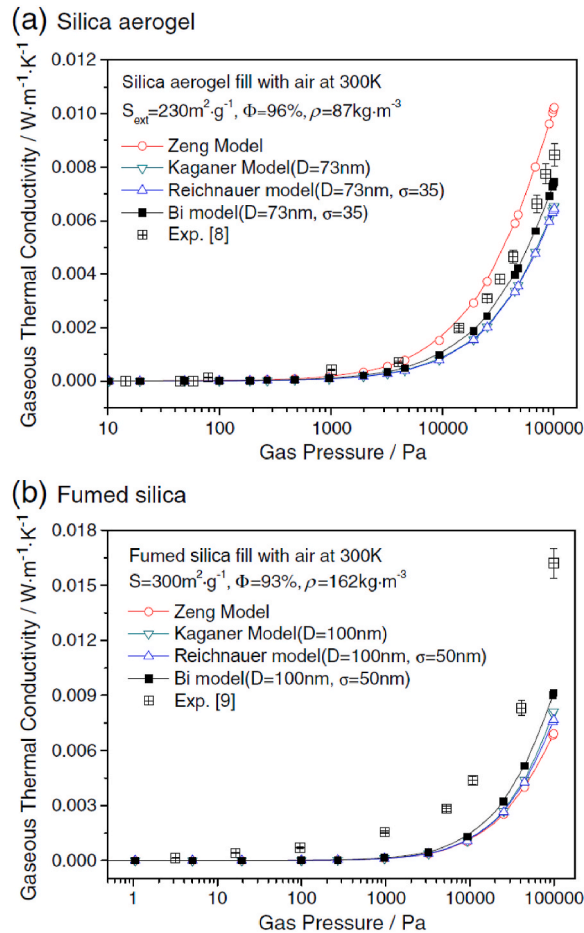


Fig. 5. Model performance under silica aerogel and fumed silica.

$$l_g = \frac{k_B T}{\sqrt{2}\pi d_g^2 p + \frac{1}{\Pi} \int_0^\infty \pi r_s^2 N_s(r_s) dr_s} = \frac{k_B T}{\sqrt{2}\pi d_g^2 p + S_s \rho / \Pi} \quad (21)$$

where, $N_s(r_s)dr_s$ represents the number density of the solid particles of radius in the range of $[r_s, r_s + dr_s]$. S_s stands for the specific surface area, defined as surface area per unit mass.

Taking the diameter of gas molecules $d_g = 3.53 \times 10^{-10}$ m = 0.353 nm and the mass of one gas molecule 4.648×10^{-26} kg into equation (21) yields

$$l_g = \frac{1}{4.01 \times 10^9 p/T + 0.25 S_s \rho / \Pi} \quad (22)$$

and

$$\lambda_g = \frac{60.22 \times 10^5 p T^{-0.5} \Pi}{4.01 \times 10^9 p/T + 0.25 S_s \rho / \Pi} \quad (23)$$

The specific surface area of aerogel S_s is determined by the porosity, pore diameter and particle diameter from experiments. λ_g is derived directly for nanoporous aerogel materials and used widely in thermal modelling studies [62].

3.8. Discussion of gaseous modelling

The performance of the four latest models (pressure dependence of gaseous thermal conductivities) has been investigated and compiled in Fig. 5. The experimental values are extracted from Bi's paper [23]. Zeng's model performs the minimal error, and Bi's model, as an improved version, is better than the Kaganer and Reichenauer models (Fig. 5a). However, the difference between the Kaganer and Reichenauer models is challenging to be identified, and both predictions are lower than the actual value.

Reichenauer model uses a more realistic pore size distribution of nanoporous materials than the Kaganer model, but surprisingly, their prediction results are almost identical. The reason may be that the effect of large pores and small pores are offset by each other in the Gaussian distribution of pore size when applying the Reichenauer model. Despite featuring symmetry distribution, the Gaussian Distribution still cannot adequately picture the pore diameter in the actual aerogel materials. In contrast, aerogels always have asymmetric pore size distributions. The Bi model achieves a better result than the Reichenauer and Kaganer models by addressing the pore size distribution simulation.

However, if one compares the results between silica aerogel and fumed silica (powder), a different phenomenon may be revealed (Fig. 5b). It is apparent that Kaganer and Reichenauer's models still give similar underestimated predictions (adapted from Ref. [23]). However, it seems that Zeng's model loses its advantages, performs worst, and gives a most underestimated result. This unexpected change cannot be explained from the current theory, and even the team that did this experiment couldn't explain the difference either.

It can be concluded that there is much research required in future that may lead to potential improvement of predictions. These may include that firstly, the different performance between different models should be investigated with different materials, e.g., silica aerogel and fumed silica (powder); Secondly, a more realistic pore size distribution is to be established for nanoporous materials. The Bi model does not truly consider the skewness of the distribution. If one can calculate equation (17) with an accurate pore size distribution, it is expected that one will get a better prediction; Thirdly, both Zeng and Bi's models have their unique advantages, but no one has yet integrated them. It is worth considering a more realistic pore size distribution with gaseous molecules modified free mean path.

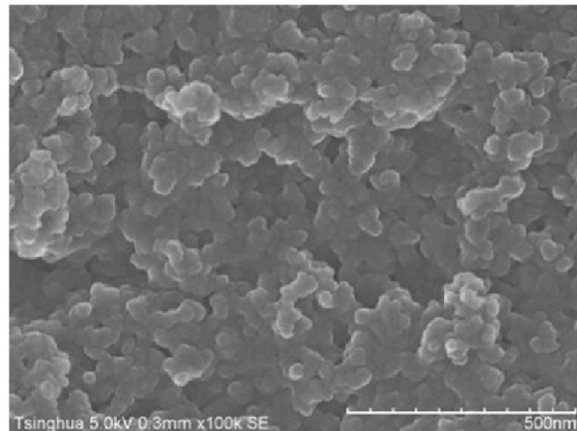


Fig. 6. Microscopic view of silica aerogel sample [63].

4. Modelling solid conductive heat transfer in aerogel composites

Aerogels are nanostructured solid networks formed by the agglomeration of nanoscale particles (Fig. 6). On the solid conductive heat transfer, the nanoscale skeleton has two effects: Firstly, because of its complex nanoscale porous structure, the solid skeleton can extend its conduction paths. Meanwhile, since the characteristic length of the solid skeleton is similar to the phonon mean free path, the heat transfer through the solid skeleton is also restricted by the size effect. Both effects reduce the heat transfer via solid skeleton.

Modelling solid conductive heat transfer in silica aerogel can be categorised into empirical, analytical, and numerical methods. An analytical method consists of a closed-form mathematical solution to the governing transport equation under the assumptions of the initial and boundary conditions. The finite difference method or finite element method is applied in a numerical model. The semi-analytical method combines numerical and closed-form solutions to solve the governing equation.

4.1. Empirical method

Fricke et al. calculates the difference in thermal conductivity before and after the gas is extracted to obtain the value of the gaseous thermal conductivity since the solid conductive heat transfer is irrelevant to the air pressure [20]. After the gas is pumped out, radiation and solid conduction remain. Although radiative heat transfer can be stopped completely when the temperature is at absolute zero (0 K), according to thermodynamic law, it is impossible to reach absolute zero using only thermodynamic means [64].

Fricke et al. measured the thermal conductivity of four opacified silica aerogels and treated the temperature as an independent variable in a vacuum environment to eliminate the radiative heat transfer. Although absolute zero is unreachable, one can calculate the intersection point of the fit line with the vertical axis, the value of solid conductivity λ_s can be estimated. In Fig. 7, the temperature-dependent variation of λ_s for various evacuated silica aerogels is shown. According to the experiment, these are around 0.009, 0.004, 0.003 and 0.002 $\text{W} \cdot \text{m}^{-1} \cdot \text{K}^{-1}$ for the different aerogels. The densities for each silica aerogel are $\rho = 75, 120, 150$ and 230 kg/m^3 respectively.

As anticipated, λ_s increases with increasing ρ . The dependences can be estimated via experiment as

$$\lambda_s \propto \rho^\alpha, \text{ with } \alpha \approx 1.5 \quad (24)$$

Throughout this experiment, one can assume that solid conductive thermal conductivity is unchanged and independent of temperature. However, this assumption is incorrect [65], which seriously compromises the credibility of this empirical model.

4.2. Analytical method

4.2.1. Periodic unit model

Zeng et al. [62] proposed a periodic cubic array model of spherical nanoparticles to mimic the solid skeleton and simulate the heat transfer with silica aerogel materials (Fig. 8). The nanoparticles are assumed to be the full density primary particles. In addition to the intersecting spheres (Fig. 9a), Zeng et al. also introduced intersecting square rods (Fig. 9b) and intersecting cylindrical rods (Fig. 9c) to represent the solid skeleton. With these assumptions, the thermal conductivities of these structures were calculated via the equivalent circuit method. Nevertheless, intersecting square rods model and intersecting cylindrical rods model does not perform well and have not been widely used. Therefore, the investigation focuses on intersecting spheres model in the next.

It is worth knowing that all possible heat transfers are included in the current Zeng's model. However, in this section, we are only interested in solid conduction. From the top to the bottom of a cell, energy is transferred in four parts, namely Q_{1g} transferred by the gas in the gap formed by two spheres in contact; Q_{1s} transferred due to solid direct contact of the spheres; Q_2 transferred from the spheres at the bottom to the spheres at the top through the gas; Q_3 transferred by the gas inside the cell, as discussed below:

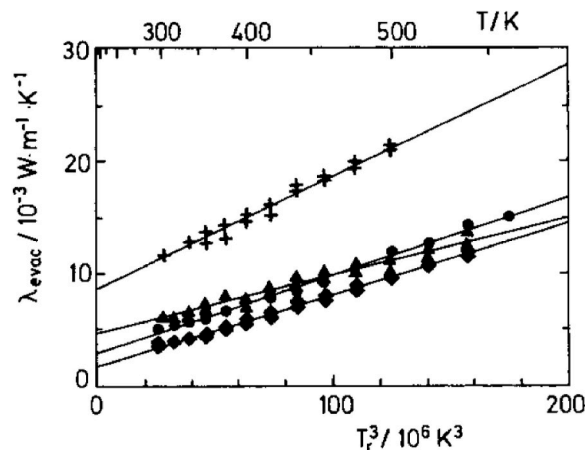


Fig. 7. Thermal conductivity λ_{evac} of various evacuated opacified monolithic SiO_2 aerogels vs T_r^{-2} . (+) $\rho = 230 \text{ kg} \cdot \text{m}^{-3}$, 2.5% soot; (▲) $\rho = 150 \text{ kg} \cdot \text{m}^{-3}$, 10% soot; (●) $\rho = 120 \text{ kg} \cdot \text{m}^{-3}$, 5% soot; (◆) $\rho = 75 \text{ kg} \cdot \text{m}^{-3}$, 5% soot [20].

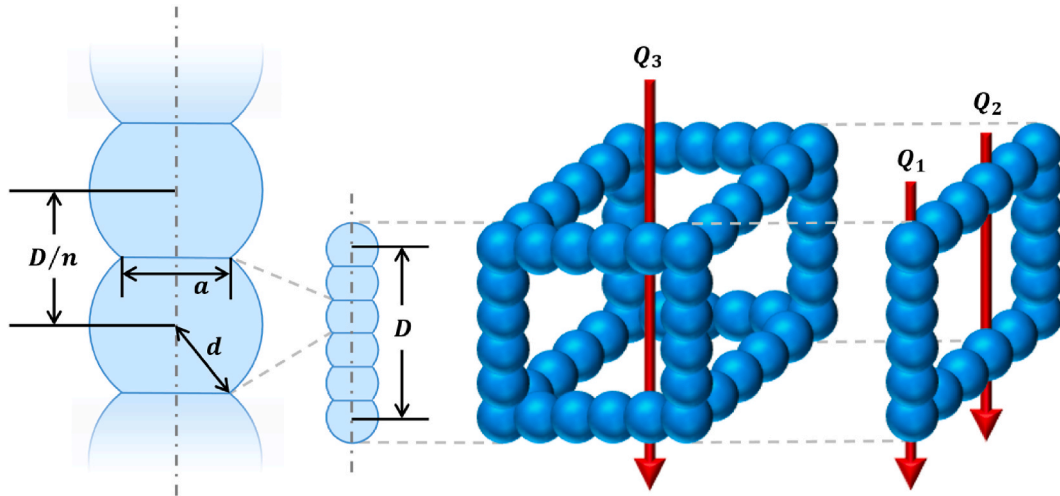


Fig. 8. Model of geometric structure of aerogel.

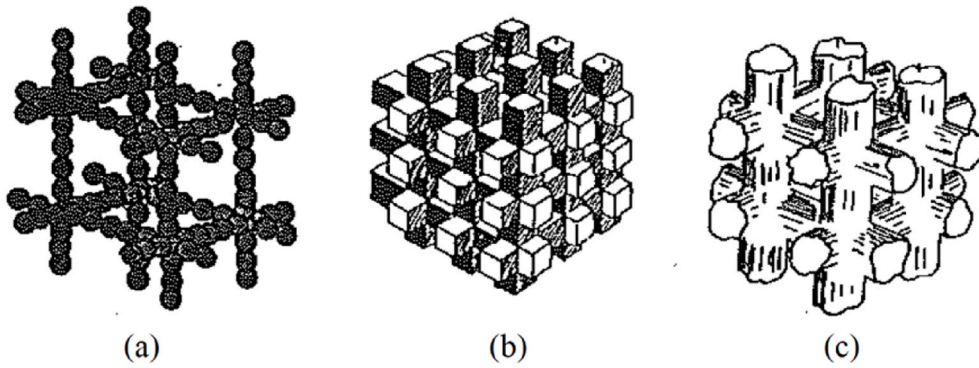


Fig. 9. Proposed skeleton of aerogel structure [62].

$$Q_{1g} = \int \frac{d}{2} \frac{(\frac{\Delta T}{n}) 2\pi x dx}{\frac{a}{2} \frac{2\sqrt{(d/2)^2 - x^2}}{k_s} + \frac{D}{n} - 2\sqrt{(d/2)^2 - x^2}} \frac{k_g}{k_s} \quad (25)$$

$$= -\frac{\pi \Delta T d k_g}{2n\beta} \left[\frac{D}{nd\beta} \ln \left\{ 1 - \frac{nd\beta}{D} \sqrt{1 - (a/d)^2} \right\} + \sqrt{1 - (a/d)^2} \right]$$

$$Q_{1s} = \frac{\pi(a/2)^2 \Delta T k_s}{D} = \frac{1}{4} \frac{\pi a^2 \Delta T k_s}{D} \quad (26)$$

$$Q_2 = \frac{(D-d)^2 \Delta T k_g}{D} \quad (27)$$

$$Q_3 = \int_0^{\sqrt{(d/2)^2 - (a/2)^2}} \frac{4(n-1)\Delta T \pi x dx}{\frac{2\sqrt{(d/2)^2 - x^2}}{k_s} + \frac{D - 2\sqrt{(d/2)^2 - x^2}}{k_g}} \quad (28)$$

$$= \frac{\pi(n-1)\Delta T d}{\beta} \left(\frac{a}{d} + \frac{D}{\beta d} \ln \frac{1 - \frac{\beta a}{D}}{1 - \frac{\beta d}{D}} - 1 \right) k_g$$

$$k_{f,s} = \frac{Q_1 + Q_2 + Q_3}{\Delta TD} = \frac{Q_{1g} + Q_{1s} + Q_2 + Q_3}{\Delta TD}$$

$$= \left\{ \frac{\pi\alpha_1^2\alpha_2^2}{4(1-\beta)} + (1-\alpha_1^2) - \frac{\pi\alpha_1^2(1-\alpha_2^2)}{2\beta^2} [\beta + \ln(1-\beta)] + \frac{\pi}{\beta} \left(\frac{1}{\sqrt{1-\alpha_2^2}} - \alpha^1 \right) \left[\frac{1}{\beta\alpha_1} \ln \frac{1-\beta\alpha_1\alpha_2}{1-\beta\alpha_1} - (1-\alpha_2) \right] \right\} k_g \quad (29)$$

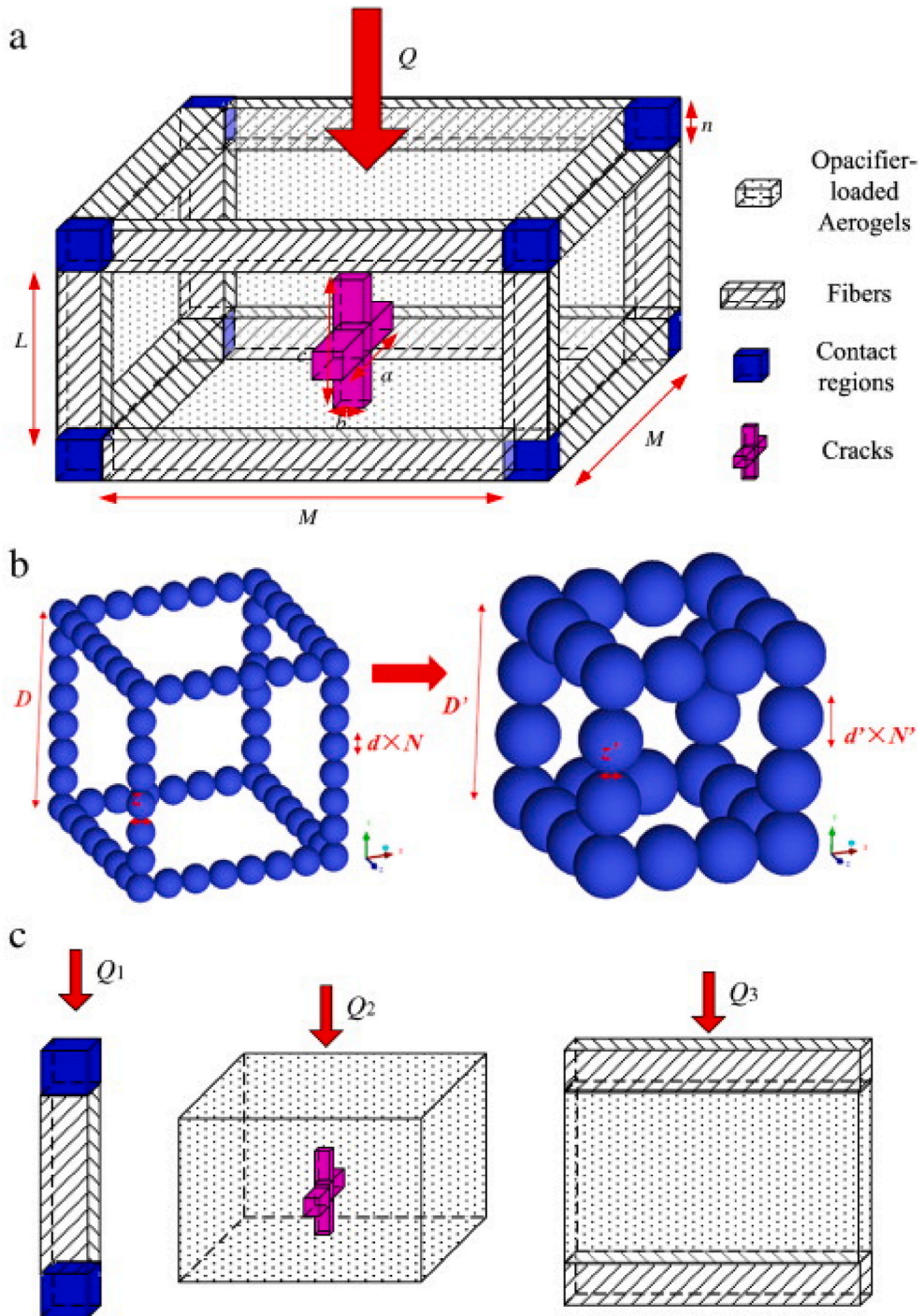


Fig. 10. Model of fibre-loaded aerogels. (a) microscale model; (b) nanoscale model; (c) heat flux path [27].

$$\alpha_1 = \frac{d}{D} \tag{30}$$

$$\alpha_2 = \frac{a}{d} \tag{31}$$

$$\beta = 1 - \frac{k_g}{k_s} \tag{32}$$

k_g (thermal conductivity of gas) and k_s (solid thermal conductivity of the rod of the cubic array) are determined on a case-by-case basis, not included in the original Zeng’s physical model.

Based on Zeng’s model, Feng et al. [65] constructed a model to describe scale heat transfer mechanisms of fumed silica-based thermal insulation composites (with fibre additives). They studied the thermal conductivity of the composite at different temperatures, including the proportion of gaseous conductive, solid conductive and radiative heat transfers. The Hamilton series model [66] was applied for the fibre additives to compute the integrated gas-solid conduction of the silica aerogel composites with non-spherical particles (fibres).

Another application of Zeng’s model for aerogel-fibre composites is Zhao’s study [67]. Zhao et al. upgraded the model of fibre-loaded silica aerogels concerning the characteristics of fibres and silica aerogels [15]. The upgraded model is constituted with a cubic array of secondary nanoparticles considering both solid and gaseous heat transfer. To calculate the heat conduction for secondary particles, Wang et al. [59] designed a fractal model to calculate the thermal conductivity of non-metallic nanoporous materials. Moreover, for solid-liquid dilute suspensions, Maxwell’s theory [68] is usually applied to estimate the effective thermal conductivity with random spherical particles when there are no particle interactions. Zhao et al. borrowed Maxwell’s theory to mimic the heat conduction between aerogel and fibre.

The Zeng model can also be applied with a multiscale system to predict the thermal conductivity of aerogel-fibre composites. Starting from the Zeng model, Lu’s designed a 3-D multiscale model [27] to analyse the influence of non-ideal structures and high temperatures on aerogel-fibre composites, as shown in Fig. 10.

With the help of the equivalent circuit method, heat transfer from the top to the bottom was considered (Fig. 10a and b). There are three types of energy transferred by conduction (Fig. 10c), namely Q_1 transfers vertically through the fibre skeleton, Q_2 transfers inside the opacifier-loaded aerogel, and Q_3 transfers from the upper fibre skeleton to the lower fibre skeleton. They can be expressed as follows:

$$Q_1 = \frac{4n^2 \Delta T}{\frac{2n}{k_c} + \frac{L}{k_f}} \tag{33}$$

$$Q_2 = \frac{M(M-b)k_{op,aer} \Delta T}{L+2n} + \frac{k_{op,aer}(M-a)b \Delta T}{L+2n} + \frac{(a-b)b \Delta T}{\frac{b}{k_g} + \frac{L+2n-b}{k_{op,aer}}} + \frac{b^2 \Delta T}{\left[\frac{c}{k_g} + \frac{L+2n-c}{k_{op,aer}} \right]} \tag{34}$$

$$Q_3 = \frac{2Mn \Delta T}{\left[\frac{L}{k_{op,aer}} + \frac{n}{k_f} \right]} \tag{35}$$

where, ΔT represents the temperature difference between the upper and lower surfaces, k_f is the fibre thermal conductivity, $k_{op,aer}$ is

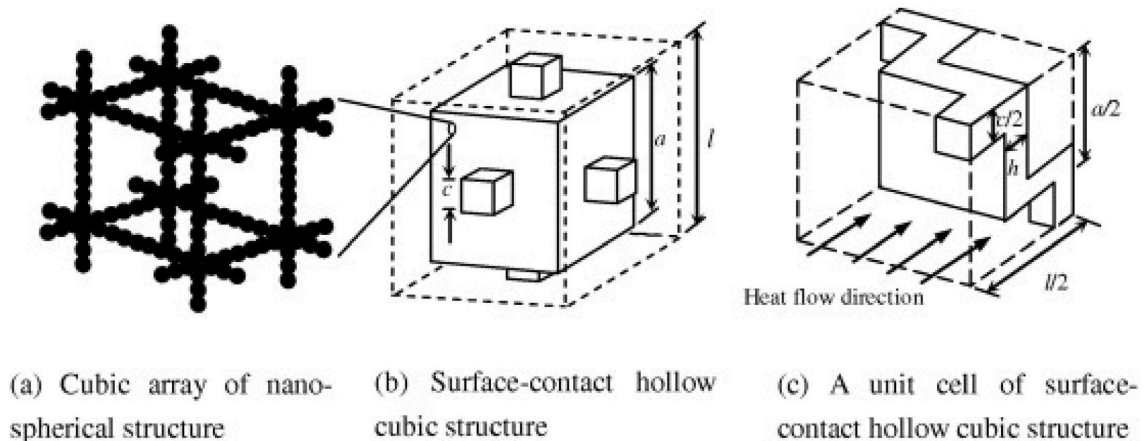


Fig. 11. Cubic array models of composite aerogel materials [69].

the coupled thermal conductivity of the opacifier-loaded silica aerogel, k_c is the thermal conductivity of the joints between interconnected fibres, which is equal to either the thermal conductivity of the gas, k_g , or the thermal conductivity of the silica aerogel, k_{aer} , depending on which component fills the joint between the interconnected fibres.

Based on Q_1 , Q_2 and Q_3 , the final thermal conductivity is:

$$k_{eff, c} = \frac{(Q_1 + Q_2 + Q_3)}{\Delta T(M + 2n)^2} (L + 2n) \tag{36}$$

In addition to fibres, xonotlite is also a common aerogel composite additive. The calcium silicates of xonotlite-type contain hollow spherical agglomerates interspersed with fibres of several hundred nanometres in diameter. A typical aerogel pore size is between 10 and 50 nm. In other words, the microstructures of xonotlite and aerogel do not adhere to the same dimensional scale and xonotlite has a much larger mean pore diameter than aerogel. As shown in Fig. 11, xonotlite-loaded aerogels can be treated as Zeng’s model of the cubic array of nano-spheres.

The spherical hollow cube model can also be used with the equivalent circuit method. By removing the sphere from a cube, Dan et al. proposed a model with a periodic unit [70] (Fig. 12 and Fig. 13). It is noteworthy that this model considers the size effect in the final thermal conductivity calculation in contrast to Zeng’s model. However, similar to Zeng’s Model, Dan’s Model was derived with the equivalent circuit method.

Four parts of the total heat flux were considered in the cube structure.

Q_1 represents the thermal conduction only through the solid structure:

$$Q_1 = \frac{\lambda_s A_1 \Delta T}{a/2} = \frac{\lambda_s \left[\frac{a^2 - \pi r^2}{2} + 2 \arccos\left(\frac{a}{2r}\right) r^2 - a \sqrt{r^2 - \left(\frac{a}{2}\right)^2} \right]}{a} \Delta T \tag{37}$$

Q_2 represents the thermal conduction only through the gas within the cell:

$$Q_2 = \frac{\lambda_g A_2 \Delta T}{a/2} = \frac{\lambda_g \pi (r^2 - a^2/4)}{2a} \Delta T \tag{38}$$

where, A_1 and A_2 are the surfaces of thermal conduction.

Q_3 and Q_4 represent the thermal conduction through gas and solid skeleton simultaneously (Fig. 12b), and are calculated as follows:

$$Q_3 = \int_{\sqrt{r^2 - a^2/4}}^{a/2} \frac{\frac{\pi}{2} x dx \Delta T}{\sqrt{r^2 - x^2} / \lambda_g + (a/2 - \sqrt{r^2 - x^2}) / \lambda_s} \tag{39}$$

where, $k = \lambda_s / \lambda_g - 1$.

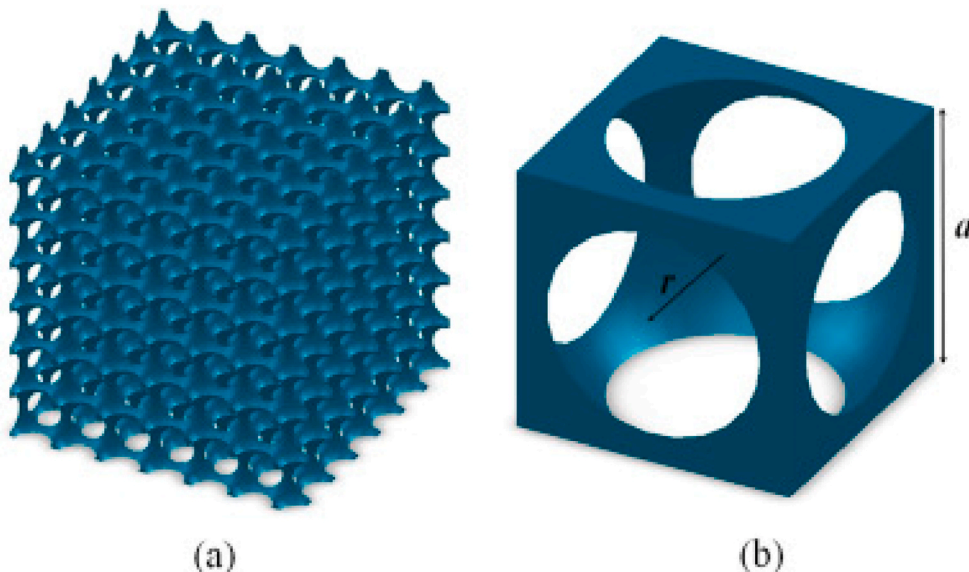


Fig. 12. (a) Overall spherical hollow structure; (b) one spherical hollow cube [70].

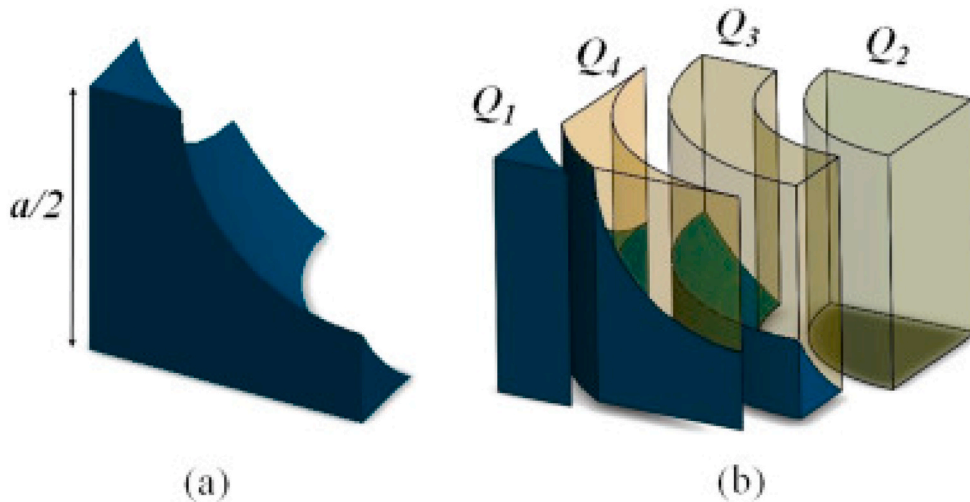


Fig. 13. (a) One unit cell (one-eighth of the spherical hollow cube); (b) exploded view of one unit cell [70].

$$Q_4 = \int_{a/2}^r \frac{\theta x dx \Delta T}{\sqrt{r^2 - x^2} / \lambda_g + (a/2 - \sqrt{r^2 - x^2}) / \lambda_s} = \int_{a/2}^r \frac{2 \cdot \arcsin\left(\frac{a/2 - \sqrt{x^2 - a^2/4}}{\sqrt{2}x}\right) x dx \Delta T}{\sqrt{r^2 - x^2} / \lambda_g + (a/2 - \sqrt{r^2 - x^2}) / \lambda_s} \quad (40)$$

where, a represents the cubic side length, r represents the radius of the spherical hollow, λ_s and λ_g are the thermal conductivity of solid and gas, respectively, and θ , θ_0 , and θ_1 are intermediate variables for integration.

The overall thermal conduction through the unit cell is:

$$\lambda_c = \frac{Q_1 + Q_2 + Q_3 + Q_4}{\Delta T \cdot a/2} = \frac{2\lambda_s \left[\frac{a^2 - \pi r^2}{2} + 2 \arccos\left(\frac{a}{2r}\right) r^2 - a \sqrt{r^2 - \left(\frac{a}{2}\right)^2} \right] + \lambda_g \pi \left(\frac{r^2}{a^2} - \frac{1}{4} \right) - \frac{\lambda_s \pi}{k^2 a} \left[kr(\cos\theta_1 - \cos\theta_0) - \frac{a}{2} \ln\left(\frac{kr\cos\theta_1 + a/2}{kr\cos\theta_0 + a/2}\right) \right] + \frac{4}{a} \int_{a/2}^r \frac{\arcsin\left(\frac{a/2 - \sqrt{x^2 - a^2/4}}{\sqrt{2}x}\right) x dx}{\sqrt{r^2 - x^2} / \lambda_g + (a/2 - \sqrt{r^2 - x^2}) / \lambda_s} \quad (41)$$

There have been several attempts to calculate the structure of the nanoporous aerogel material using regular structures, such as cubic arrays of intersecting spheres and spherical hollow cubes. With regular structures, heat transfer analysis within the material is simplified, but such analyses overlook the complex microstructural properties of aerogel material.

4.2.2. Fractal model

Fractal structures are often observed in nanoporous materials, such as silica aerogels. When constructing the physical model, the fractal theory can be applied to simulate the irregular characteristics of the aerogel better. Xie et al. made a meaningful attempt [24] to integrate the intersecting spheres and fractal elements. A new fractal interlocking sphere model combines the classic Sierpinski sponge with the intersecting sphere structure (Fig. 14). The size effect on gas conduction and solid conduction is also a part of the consideration in a fractal-intersecting sphere model.

Cheng and Hsu [71] used equivalent circuit method to predict the effective thermal conductivity of the fractal-intersecting sphere model:

$$k_{ae}^1 = 4k_{unit} \left(\frac{1 - \gamma}{2} \right)^2 + \frac{4k_{unit} k_g \gamma (1 - \gamma)}{2k_g (1 - \gamma) + 2k_{unit} \gamma} + k_g \gamma^2 \quad (42)$$

$$k_{ae}^n = 4k_{ae}^{n-1} \left(\frac{1 - \gamma}{2} \right)^2 + \frac{4k_{ae}^{n-1} k_g \gamma (1 - \gamma)}{2k_g (1 - \gamma) + 2k_{ae}^{n-1} \gamma} + k_g \gamma^2 \quad (43)$$

where, k_g is the gaseous thermal conductivity, and k_{unit} is the effective thermal conductivity of primary unit cell of fractal-intersecting sphere model (Fig. 14c), which can be expressed as:

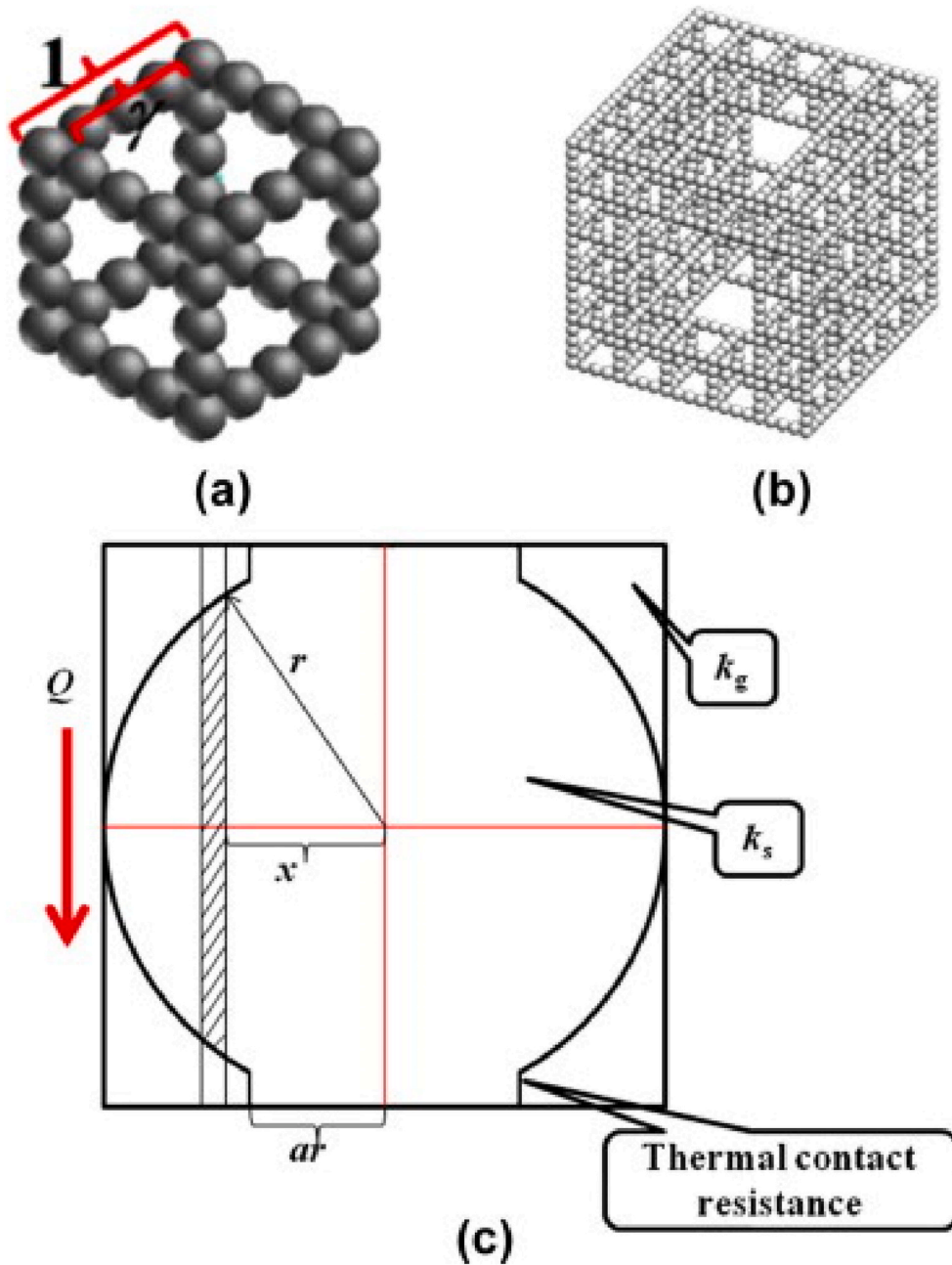


Fig. 14. (a) One cubic array cube (b) overall structure (c) one unit cell [24].

$$k_{unit} = \left\{ \frac{-2k_s^2 k_g}{(k_g - k_s)^2} \ln \left(1 + M \left(\frac{k_g}{k_s} - 1 \right) \right) - M \frac{2k_g k_s}{k_s - k_g} \right\} + a^2 k_s \tag{44}$$

where, $M = \cos(\arcsin(a))$, a is the ratio of contact resistance length to the diameter of the particle.

4.3. Numerical method

4.3.1. Periodic and fractal model

Spagnol et al. [72] built a two-dimensional periodic fractal pattern to determine the heat flux and temperature field by solving the steady heat conduction equation for solid-gas coupling heat conduction with Fourier's Law.

In the Spagnol model, periodic models were designed with elementary Von Koch snowflakes. These geometries (Fig. 15) allow the modelling of the complex structure's different pore sizes, fractality, and isotropy. Based on two parameters: density and tortuosity, the

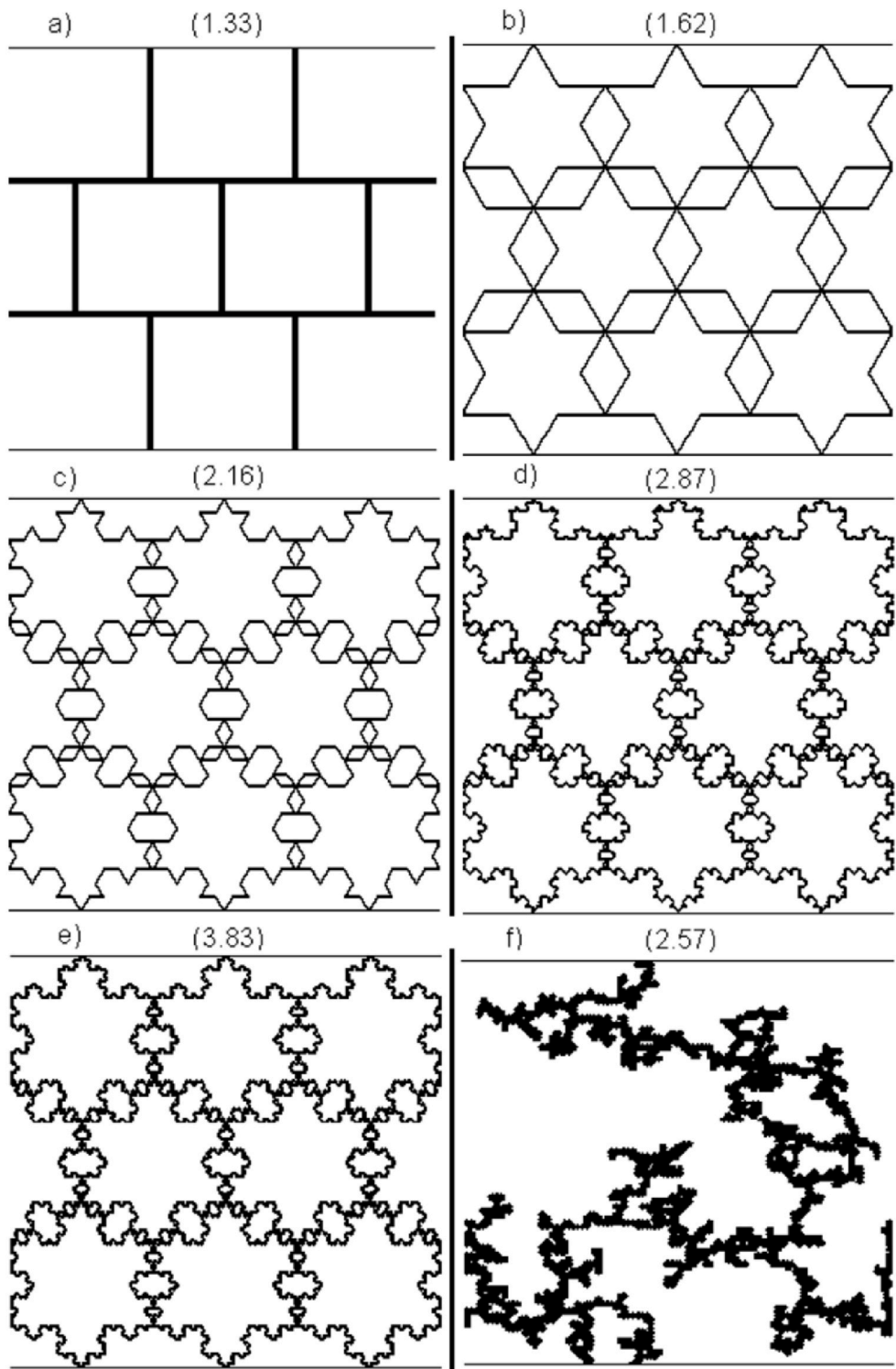


Fig. 15. a) brick wall model, (b)–(e) periodic Von Koch snowflakes at different order, and f) 2-D DLCA model [72].

numeric model of effective thermal conductivity was built by Spagnol.

At the steady-state conditions, Spagnol et al. solved the equation of $\nabla(-k_i \times \nabla T_i) = 0$ for both solid and gas phases via the 2-D heat diffusion equation. For the top (the hot side) and bottom side (the cold side), every place was assumed with the same temperature and flux, and the Dirichlet boundary conditions were imposed. The left and right sides are the adiabatic sides for heat transfer. Finally, the

finite differences method can be used to solve $\nabla(-k_i \times \nabla T_i) = 0$ (Fig. 16).

$$k_{effX} = \frac{X}{Y \times (T_{hot} - T_{cold})} \times \int_0^Y \left(-k_i \times \frac{\partial T_i}{\partial x_i} \right) dy \tag{45}$$

where, X is the length of the vertical axis, and Y is the length of the horizontal axis.

For the original model, Spagnol et al. made the following assumptions:

- (1) no heat convection between different phases (gas and solid).
- (2) temperature and heat flux change continuously at the interface between different phases.
- (3) The Kaganer model is used to analyse non-equilibrium effects with the rarefied gas.

One of the most severe drawbacks of this model is no consideration of the size effect.

Knudsen number is close to 1 since the free mean path of gas molecules is similar to the average pore size of silica aerogel materials.

To take size effect into consideration of calculating thermal conductivity, Bi et al. [61] proposed an improved Spagnol model with two more assumptions and expanded the original model to three-dimension, as shown in Fig. 17, to make a more accurate prediction.

To calculate the solid-gas coupling heat conduction of aerogels, Spagnol used the steady-state heat diffusion equation (46) as the numerical method,

$$\frac{\partial}{\partial x} \left(\lambda_i \frac{\partial T}{\partial x} \right) + \frac{\partial}{\partial y} \left(\lambda_i \frac{\partial T}{\partial y} \right) + \frac{\partial}{\partial z} \left(\lambda_i \frac{\partial T}{\partial z} \right) = 0 \tag{46}$$

where, λ_i can be λ_g (gaseous thermal conductivity) or λ_s (solid thermal conductivity) respectively.

The first extra assumption compared to the original Spagnol's model is introducing the size effect in solid heat conduction. Applying the approximation $\lambda_s \approx \lambda_{backbone}$ of in equation (46), one can calculate λ_s by the kinetic theory:

$$\lambda_{backbone} = \frac{C_V v \lambda}{3} \tag{47}$$

where, C_V is the volume-specific heat, v is the mean sound velocity in the aerogel backbone, and λ the average interatomic spacing in the aerogel backbone, determined by the diameter of aerogel particles and the space between aerogel particles.

Compared to the original Spagnol's model, Bi introduced the size effect of heat conduction in the gas phase as the second extra assumption. Total three equations are introduced with this assumption:

$$D \approx \frac{4V_{pore}}{S_{ext}} = \frac{4}{S_{ext}} \left(\frac{1}{\rho} - \frac{1}{\rho_s} \right) \tag{48}$$

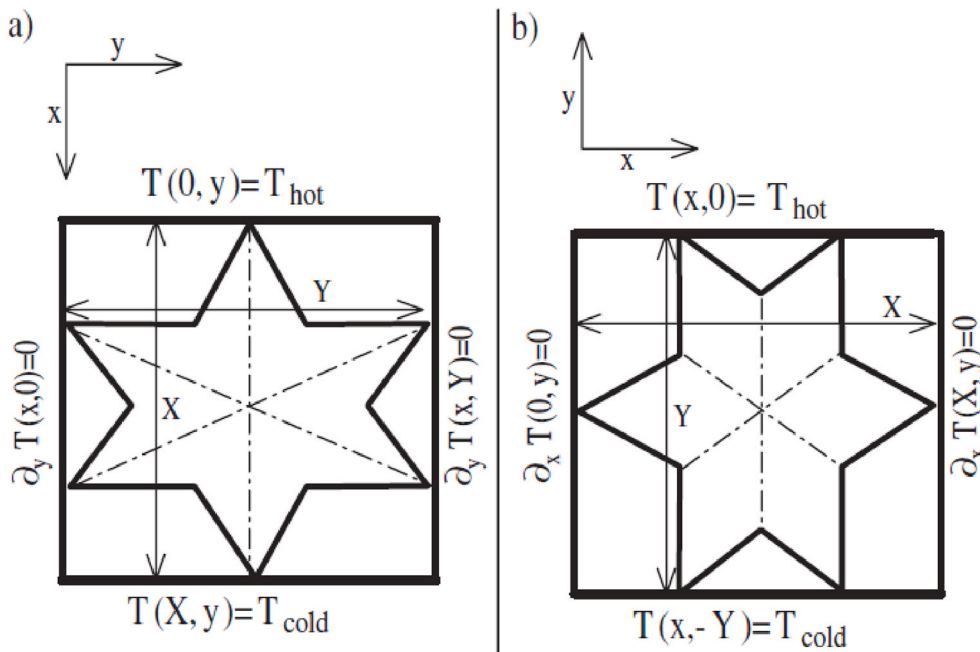


Fig. 16. Geometric parameters of one Von Koch snowflake; a) to calculate k_{effX} and b) to calculate k_{effY} [72].

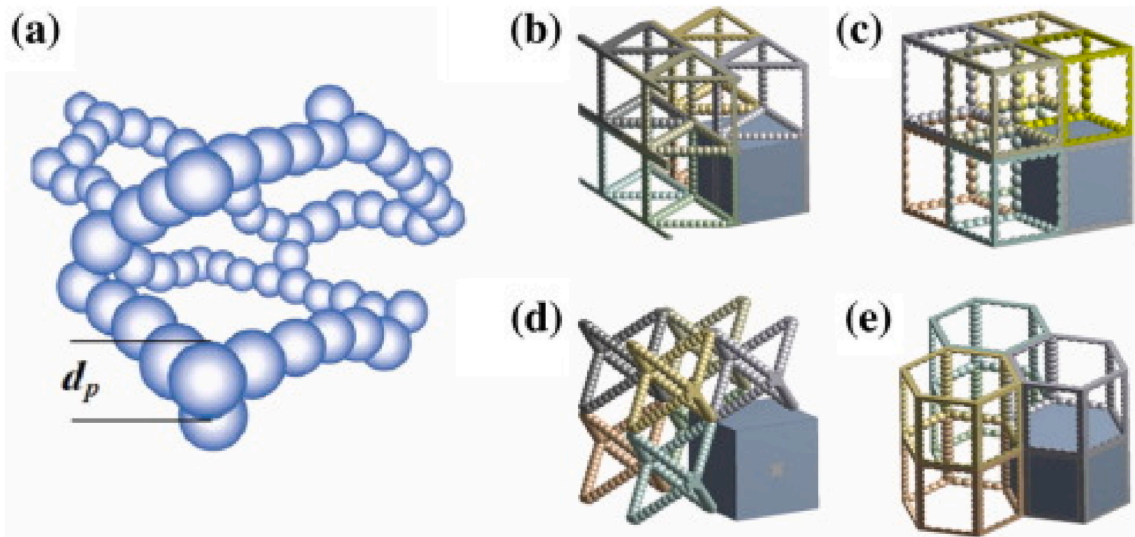


Fig. 17. Schematic of base-catalysed aerogel structures. (a) Aerogel backbone. (b) Regular triangular prism. (c) Cube. (d) Octahedron. (e) Regular hexagonal prism [61].

$$d_p \approx \frac{6}{S_{ext}\rho_s} \tag{49}$$

$$\Phi = 1 - \frac{\rho}{\rho_s} \tag{50}$$

where, V_{pore} is the pore volume, S_{ext} is the external specific surface area of aerogel, ρ is the aerogel density, ρ_s is the density of aerogel solid phase, and Φ is the aerogel porosity.

Solving (48), (49) and (50) together, then Bi got the equation $d_p = \frac{3}{2}D\frac{1-\Phi}{\Phi}$ and finally obtained the relation between the pore size D and particle size d_p of the aerogel [61].

4.3.2. Aggregation model

Aerogels are generally referred to as lightweight solid nanoscale materials, which are made up of nanoparticles aggregating to form solid networks that are nanostructured. To generate the random aggregated nanoparticle structure, the following three basic colloidal aggregation processes have been implemented, diffusion-limited cluster aggregation (DLCA) [73], ballistic cluster aggregation (BCA), and reaction-limited cluster aggregation (RLCA) [74]. In comparison to BCA, DLCA and RLCA are better for modelling the structure of silica aerogel. The DLCA process happens when nanoparticles adhere to each other upon collision if there is no significant repulsive force between them. The RLCA process occurs when there is a significant but not overwhelming interaction between the nanoparticles [25].

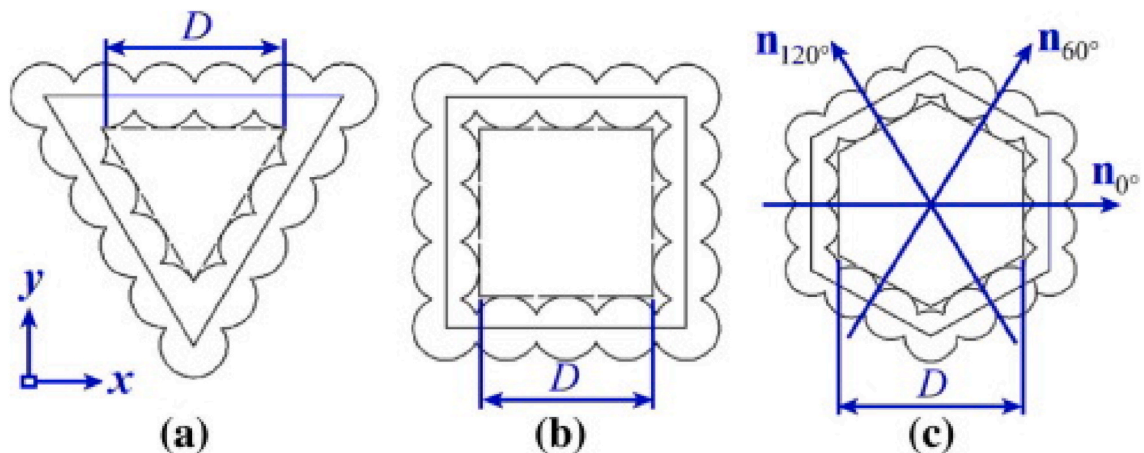


Fig. 18. Definition of pore size of the ordered structures. (a) Triangular. (b) Cubic. (c) Hexagonal [61].

The authors of the above articles have compared the advantages and disadvantages of various methods for generating aerogels in detail; however, they have not addressed the topic of heat transfer and have remained at the level of physical structure. Zhao et al. [28] applied the DLCA model to generate a 3-D random structure of aerogel material used to predict the effective thermal conductivity, including radiation and conduction.

Every elementary cubic unit in the material was determined by DLCA generation, including the gas or nanoparticles. Inside a cubic box of side length N_1 , as shown in Fig. 19a, heat transfer simulation was calculated with gas or nanoparticles. The heat transfer was assumed for the cubic box itself through 6 adjacent cubic boxes, as shown in Figure 19b.

The 3-D steady-state heat diffusion equation is:

$$\nabla(k_c \nabla T - q''_r) = 0 \tag{51}$$

Subject to isothermal boundary conditions on the left and right faces and adiabatic boundary conditions on the other four faces (Fig. 18a), then,

$$T(0, y, z) = T_h \tag{52}$$

$$T(L, y, z) = T_c \tag{53}$$

$$\frac{\partial T}{\partial y}(x, 0, z) = \frac{\partial T}{\partial y}(x, L, z) = \frac{\partial T}{\partial z}(x, y, 0) = \frac{\partial T}{\partial z}(x, y, L) = 0 \tag{54}$$

where ∇ is the 3-D gradient operator, q''_r is the radiative heat flux, L is the insulation thickness or the cubic box side length, T_h is the hot side temperature, T_c is the cold side temperature, and k_c is the conductive thermal conductivity of the material in the cubic element, which is k_g for gases or k_s for the equivalent solid cubic element consisting of the nanoparticle and the gap gases between adjacent nanoparticles.

The calculation started from the hot side (0, y, z) to the cold side (L, y, z). The heat diffusion equation (51) was solved with a finite volume method under the boundary conditions in equation (52), equation (53) and equation (54) to calculate the steady-state temperature field in the cubic domain $T(x, y, z)$.

Similar to Zhao's study, Zhu et al. proposed an improved DLCA to generate the structure of silica aerogel [26], which is shown in (Fig. 20a). With a small gap between adjacent particles, all particles are arranged in rows (Fig. 20b). It is possible to describe the structure of silica aerogels with the help of the generated 3-D model. Based on that unique structure, lattice nodes can easily enclose the gap between two particles.

Zhao's study solved the energy governing equation with the finite difference method (FDM). However, FDM, Finite element method (FEM) and Finite volume method (FVM) are macroscopic numerical methods used for the continuous medium in classical

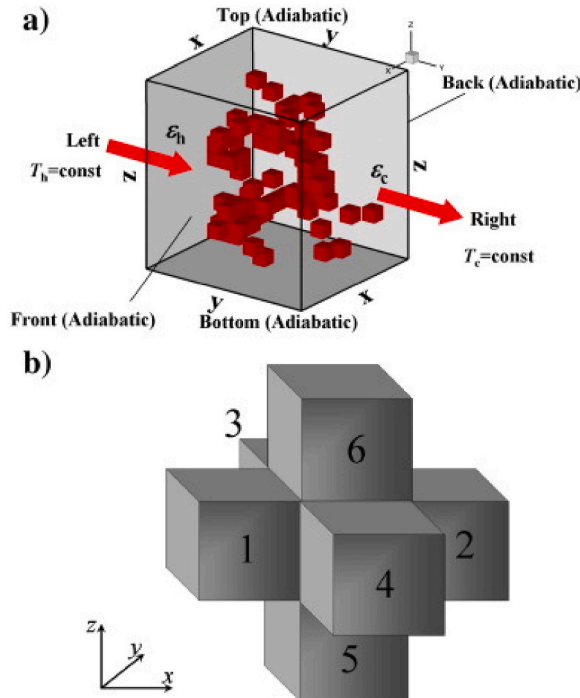


Fig. 19. (a) Boundary conditions; (b) lattice face-contacting six neighbouring lattices [28].

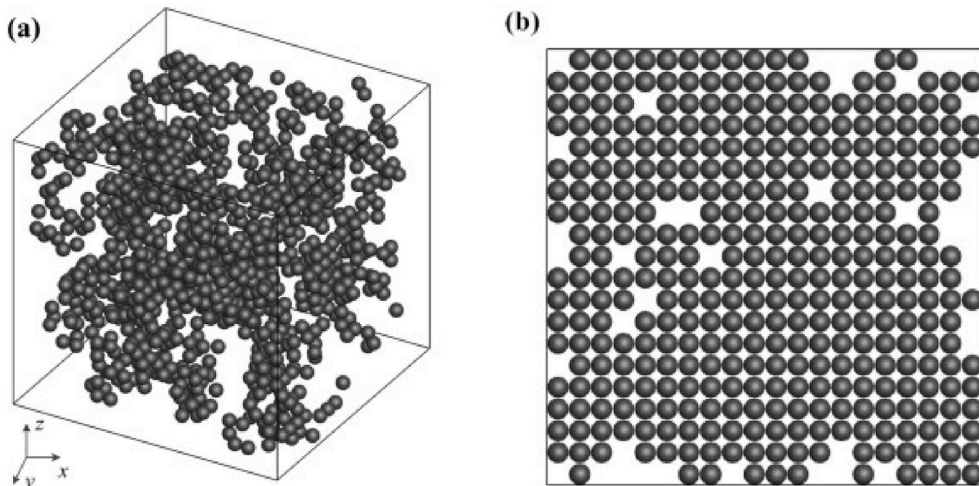


Fig. 20. A improved DLCA generation result with a (93% porosity) generated (a) the overall structure; (b) the 2-D slice [56].

Computational Fluid Dynamics (CFD) methods. Strictly speaking, FDM, FEM and FVM cannot be applied to the nanoporous aerogel material. The Lattice Boltzmann Method (LBM) should be better. Multiple particle interactions are easily achieved using LBM and complex geometric boundary conditions. Therefore, over the decades, LBM has been successfully used as a mesoscopic approach to address heat transfer problems in micro and nanoporous materials [75].

There are advantages and disadvantages of periodic and aggregation models (Table 2). Therefore, it is essential to develop a strategy of taking advantage of two models for an accurate prediction. By doing so, one may obtain the randomness of the pore size and the solid skeleton distribution and calculate the effective thermal conductivity with analytical methods by considering each nano (primary) particle and even the nano-secondary particle. In addition, as discussed in the previous section 3.7, the randomness of pore sizes can be created more realistic by considering the actual distribution of nanopore sizes and achieving by the improved aggregation (DLCA) algorithm.

4.4. Discussion of solid conduction modelling

As one of the major heat transfer approaches in porous materials, solid heat conduction has been the focus of researchers trying to simulate. At first, when scientists had minimal knowledge about the microstructure of nanoporous materials such as aerogel, only empirical models could be obtained by experiments. Fricke et al. are the first group of recorded scientists who performed the repeated vacuumed experiments with the controlled variable of different environmental temperatures. Supported by experimental results, Fricke et al. assumed that the effective thermal conductivity and environmental temperature have a linear relationship; hence, the value of y-intercept in Fig. 7 is the thermal conductivity of solid conduction only. The idea of Fricke's experiment is instructive to later scientists, but the assumptions for making the conclusions are flawed. Details are referred in Section 4.1.

Due to the unremitting pursuit of the accuracy of prediction results, analytical modelling was performed by the later scientists with more advanced microscopes and tomography equipment. The initial thought is to treat the solid skeleton as a periodical structure, such as a cubic array by Zeng et al. Lu improved Zeng's work by considering the microstructure as two scales: microscale and nanoscale achieve a more realistic physical modelling. Dan improved Zeng's model from the other direction and treated the unit cell as a spherical hollow cube. All the periodic physical models are applied with equivalent circuits method to compute heat transfer. In pursuit of the simulation of more complex microstructures, fractal models were introduced by Xie, Cheng and Hse. However, although the idea of fractals adds endless complexity to physical models, fractal models are still overly idealised that ignore the irregularities of the reality of materials.

The latest analytical model applies the idea of aggregation. Although the physical structures of the aggregation models generated

Table 2
The advantages and disadvantages of existing periodic and aggregative physical models.

	Advantages	Disadvantage
Current aggregation models	<ol style="list-style-type: none"> 1) More in line with the randomness of the skeleton of nanoporous materials 2) Non-uniform pore size distribution 	<ol style="list-style-type: none"> 1) No analytical method used to calculate thermal conductivity 2) No consideration of nano secondary particles 3) lack of consideration of the more complex actual pore size distribution
Current periodic models	<ol style="list-style-type: none"> 1) Easy to use analytical methods to calculate accurate thermal conductivity 2) Consideration of nano secondary particles in some models 	<ol style="list-style-type: none"> 1) Assumption of uniform pore size distribution, which is not realistic 2) Assumption of periodic distribution of solid skeleton, which is not realistic

by different random seeds are different, scientists can obtain the most realistic microstructure and achieve the most accurate prediction of thermal conductivity, without the tomography, by repeating the experiment and taking the average.

5. Modelling radiative heat transfer of aerogel composites

Radiative heat transfer is the heat transfer from a heated object to a cold object via the radiant energy emitted from the heated object. The radiant energy, known as radiation, can be absorbed, reflected, or scattered when it transfers through the media. Rosseland diffusion approximation is applied to predict the radiative heat flux of aerogel substances.

However, silica aerogel has a slight absorption coefficient in the range of 3 μm –8 μm , where radiation transfers a large amount of energy [76]. At room temperature, radiative heat transfer only contributes a small proportion of the effective thermal conductivity of silica aerogel, but this proportion will increase rapidly with the increasing temperature. Hence, opacifiers, such as carbon or TiO_2 , are added to silica aerogel materials to reduce thermal radiation transfer by efficiently absorbing and scattering the radiation. As a theory for particle scattering, Mie's theory is the most commonly used and fundamental algorithm, and it is unrivalled in terms of particle scattering issues. In this theory, Maxwell equations can determine radiation characteristics for spherical particles.

The unique three-dimensional network structure of silica aerogel causes low strength and brittleness, and it is often fragmented, which could be its most significant disadvantage. In most studies, researchers add fibres to improve the mechanical behaviour of aerogel. Fibres are mixed chemically and mechanically into the silicon aerogel skeleton to produce a composite aerogel with the fibre reinforcement method. There are currently a variety of inorganic fibres, such as glass fibres, mullite fibres, composite fibres, carbon fibres and polymer fibres.

To compute the total extinction coefficient of aerogel composites, researchers need to calculate the extinction factors of aerogel and additives separately and add them together. Aerogel extinction factors are calculated by treating the silica aerogel material as a homogeneous medium without considering its nanoporous structure. Radiation calculation of aerogel is based on the material's overall performance and not on nanoscale characteristics. For additives, due to the characteristics of absorption and scattering of radiation, researchers need to adopt different methods and ideas for different shapes of additives, such as sphere and long cylinder.

These various shapes of additives complicate the calculation of radiation. In particle scattering issues raised by additives, the Mie scattering theory [31] is the most accurate as well as the commonly used method. Regarding fibrous additives, Lee and Cunnington developed Mie's theory to make it applicable to non-spherical additives by calculating the total radiative properties of fibres from integrating each fibre's radiative properties. As an alternative, van de Hulst's Anomalous Diffraction Theory (ADT) can also be applied to approximate Einstein's Mie theory. It can predict spheres, spheroids and cylindrical extinction efficiency within a reasonable range.

5.1. Modelling radiative conductivity of aerogel

Practically speaking, the optical thickness of nanoporous materials or fibre-based materials is typically substantial. Hence, the radiative thermal conductivity can be expressed based on the Rosseland diffusion approximation [30]:

$$\lambda_r = \frac{16n^2\sigma T^3}{3\rho K_{e,m}} \quad (55)$$

where, σ is the Stefan–Boltzmann constant, n is the mean refractive index, T is the absolute temperature, ρ is the density of materials and $K_{e,m}$ is the specific extinction coefficient.

5.2. Modelling radiative conductivity of additives (opacifier particles and fibres)

5.2.1. Radiative conductivity of spherical additives

Assuming that the opacifiers are spherical particles, according to Mie's theory [31], the extinction factors of a single particle could be calculated by:

$$Q_{e\lambda} = \frac{C_{e\lambda}}{\pi r^2} = \frac{2}{\chi^2} \sum_{n=1}^{\infty} (2n+1) \text{Re}[a_n + b_n] \quad (56)$$

where, Re is the symbol of the real part, r is the particle radius, χ is the size factor defined as $\pi D/\lambda$, where $D = 2r$ is the particle diameter, $Q_{e\lambda}$ is the spectral extinction factor, a_n and b_n are the Mie coefficients which are functions of particle's complex refractive index ($n - ki$). Using the above equation, it is necessary to first calculate the particle's complex refractive index before calculating the scattering and extinction factors.

Mie assumed that the distribution of opacifier particles in aerogel composites is sparse; hence, the scattering of every particle is independent. One can calculate the total radiative properties of opacifier particles once one gets the radiative characteristic of each particle by summing the contribution of all opacifier particles.

Following is the relationship between total extinction coefficient and extinction factor for each individual particle:

$$\sigma_{e\lambda} = \frac{\pi}{4} \sum_{i=1}^n D_i^2 N_i Q_{e\lambda,i} = \frac{3}{2} \sum_{i=1}^n Q_{e\lambda,i} \frac{f_{v,i}}{D_i} = \frac{3}{2} Q_{e\lambda} \frac{f_v}{D} \quad (57)$$

where, N_i is the particle number density for the i th particle, n is the number of different particle sizes, $f_{v,i}$ is the volume fraction for the i th particle and given by $f_{v,i} = \pi D_i^3 N_i/6$.

5.2.2. Radiative conductivity of fibrous additives

Like Mie's theory, one can calculate the radiative properties of fibres once one gets the radiative characteristic of each fibre by calculating integrating the total extinction coefficients of each fibre [32].

$$\{\bar{\sigma}_{e\lambda}\} = \int_{\omega_{f1}}^{\omega_{f2}} \int_{\xi_{f1}}^{\xi_{f2}} \int_0^{\infty} 2r\{Q_{e\lambda}\}N(r(\mathbf{R}_f))drd^2F \quad (58)$$

where, d^2F and $N(r(\mathbf{R}_f))$ are the orientation distribution and number size distribution, and the limits of integration (ξ_{f1} , ξ_{f2} , ω_{f1} , ω_{f2}) denote the range of the angular orientation of fibres. For the case in which fibres are randomly oriented, the equation becomes:

$$\{\bar{\sigma}_{e\lambda}\} = \frac{2f_v}{\pi r} \int_0^{\pi/2} \{Q_{e\lambda}(\theta)\} \cos\theta d\theta \quad (59)$$

The incident angle θ becomes 90° when fibres are located perpendicular to the direction of heat flow, and the equation becomes:

$$\bar{\sigma}_{e\lambda} = \int_{\omega_{f1}}^{\omega_{f2}} \int_{\xi_{f1}}^{\xi_{f2}} \int_0^{\infty} 2r\{Q_{e\lambda}\}N(r(\mathbf{R}_f))drd^2F = \frac{2f_v}{\pi r} Q_{e\lambda} \quad (60)$$

The Mie theory is feasible but inefficient since the calculation of the infinite series. Anomalous diffraction theory (ADT) [77] is an acceptable approximation to Mie theory which can predict the extinction efficiency of spheres, spheroids, and cylinders. Furthermore, based on the incident angle, fibre geometry, and optical properties, ADT provides an elegant mathematical model of fibre extinction efficiency.

5.3. Discussion of radiative heat transfer modelling

Due to the low absorption of silica aerogel within some wavelengths, the Rosseland diffusion approximation, which can only be applied to thick opaque media, is not a satisfactory solution to calculate the radiation of porous medium as silica aerogel. To address the limitation of Rosseland diffusion approximation, a formulation for the coupling of conduction and radiation in a porous medium with arbitrary thickness has been proposed by Zeng et al. [78] Besides.

As the latest and most complete theory, Mie's theory is the accurate method to calculate the globule extinction coefficient. Lie et al. [79] confirmed that Mie's theory was in relatively good agreement with the retrieved data.

Unlike solid and gaseous conduction, radiation and global extinction coefficients are irrelevant to pressure but positively correlate with temperature [79]. When silica aerogel composites work in an ordinary low temperature, the percentage of radiative heat transfer compared to the effective heat transfer is between 0.9% (290 K) and 2.1% (290 K). This percentage increases rapidly when the working temperature goes up, reaching 9.2% at 690 K and 23.8% at 990 K. In this circumstance, the radiation must be considered to avoid noticeable errors.

6. Conclusions

The modelling of aerogels' gaseous, solid and radiative heat transfers has been comprehensively reviewed to examine their principles, application fitness and limitations and identify the research needs. Some significant conclusions can be drawn as follows:

- 1) All the current work only concentrated on one way of heat transfer. No one considered the problem at the level of effective thermal conductivity with a complete heat transfer model of silica aerogel materials, the lack of which does not match the widespread use of silica aerogels.
- 2) There have been two types of models of gaseous thermal conductivity in silicon aerogel composites: empirical and theoretical models. All the latest gaseous models came from gas kinetic theory, which could be divided into two branches: firstly, a gaussian distribution of pore sizes was applied to obtain a more accurate microstructure of silica aerogels and secondly, a model was proposed considering the influence of solid skeletons on the mean free path of gas molecules. Integration of a more realistic distribution of pore diameters and adjusting the mean free path of gas molecules might be the breaking point of gaseous modelling in the future.
- 3) Modelling solid conductive heat transfer in silica aerogel could be categorised into empirical, analytical and numerical methods. Periodic and aggregated models were two major solid models. The aggregated models considering secondary particles represented the state-of-the-art of solid modelling works. However, even the aggregated model could not construct a physical model comparable to the actual microstructure of materials. A more advanced machine learning algorithm with 3D scan results might be applied to improve the fidelity of physical models.
- 4) Rosseland diffusion theory empowered researchers to calculate the radiative heat transfer through silica aerogels. Considering the influence of additives, Mie's theory has been used to compute the extinction factors of spherical opacifier particles, extended to the calculation of fibrous additives together with the Anomalous diffraction theory.

Declaration of competing interest

The authors declare that they have no known competing financial interests or personal relationships that could have appeared to influence the work reported in this paper.

Acknowledgement

The project leading to this paper has received funding from the European Union's Horizon 2020 research and innovation programme under Grant Agreement No. 869898.

References

- [1] L.W. Hrubesh, Aerogel applications, *J. Non-Cryst. Solids* 225 (1998) 335–342.
- [2] M. Schmidt, F. Schwertfeger, Applications for silica aerogel products, *J. Non-Cryst. Solids* 225 (1–3) (1998) 364–368.
- [3] R. Baetens, B.P. Jelle, A. Gustavsen, Aerogel insulation for building applications: a state-of-the-art review, *Energy Build.* 43 (4) (2011) 761–769.
- [4] M. Bouquerel, T. Duforestel, D. Baillis, G. Rusaouen, Heat transfer modeling in vacuum insulation panels containing nanoporous silicas—a review, *Energy Build.* 54 (2012) 320–336.
- [5] M. Reim, W. Körner, J. Manara, S. Korder, M. Arduini-Schuster, H.-Ebert, J. Fricke, Silica aerogel granulate material for thermal insulation and daylighting, *Sol. Energy* 79 (2) (2005) 131–139.
- [6] D.M. Smith, A. Maskara, U. Boes, Aerogel-based thermal insulation, *J. Non-Cryst. Solids* 225 (1–3) (1998) 254–259.
- [7] E. Bardy, J. Mollendorf, D. Pendergast, Thermal conductivity and compressive strain of foam neoprene insulation under hydrostatic pressure, *Journal of physics. D, Applied Physics* 38 (20) (2005) 3832–3840.
- [8] N.A. Zubair, E. Abouzari-Lotf, M. Mahmoud Nasef, E.C. Abdullah, Aerogel-based materials for adsorbent applications in material domains, *E3S web of Conferences* 90 (2019) 1003.
- [9] P. Arabkhani, A. Asfaram, Development of a novel three-dimensional magnetic polymer aerogel as an efficient adsorbent for malachite green removal, *J. Hazard Mater.* 384 (2020), 121394.
- [10] H. Hu, N. Chen, W. Wei, H. Li, Z. Jiang, Y. Xu, J. Xie, The effect of solvent parameters on properties of iron-based silica binary aerogels as adsorbents, *J. Colloid Interface Sci.* 549 (2019) 189–200.
- [11] J. Xiao, Y. Tan, Y. Song, Q. Zheng, A flyweight and superelastic graphene aerogel as a high-capacity adsorbent and highly sensitive pressure sensor, *J. Mater. Chem.* 6 (19) (2018) 9074–9080.
- [12] K.G. Kirste, S. Laassiri, Z. Hu, D. Stoian, L. Torrente-Murciano, J.S.J. Hargreaves, K. Mathisen, XAS investigation of silica aerogel supported cobalt rhenium catalysts for ammonia decomposition, *Phys. Chem. Chem. Phys.* 22 (34) (2020) 18932–18949.
- [13] T. Yousefi Amiri, J. Moghaddas, Cogeled copper–silica aerogel as a catalyst in hydrogen production from methanol steam reforming, *Int. J. Hydrogen Energy* 40 (3) (2015) 1472–1480.
- [14] S. Tajik, B. Nasrnejad, A. Rashidi, Surface modification of silica-graphene nanohybrid as a novel stabilizer for oil-water emulsion, *Kor. J. Chem. Eng.* 34 (9) (2017) 2488–2497.
- [15] B.C. Dunn, P. Cole, D. Covington, M.C. Webster, R.J. Pugmire, R.D. Ernst, E.M. Eyring, N. Shah, G.P. Huffman, Silica aerogel supported catalysts for Fischer–Tropsch synthesis, *Appl. Catal. Gen.* 278 (2) (2005) 233–238.
- [16] Aerogels edited, in: J. Fricke (Ed.), *Proceedings in Physics*, vol. 6, Springer-Verlag, 1986, pp. 4–5. *MRS Bull* 1986;11(6).
- [17] L.W. Hrubesh, R.W. Pekala, Thermal properties of organic and inorganic aerogels, *J. Mater. Res.* 9 (3) (1994) 731–738.
- [18] H. Zhang, W. Fang, Z. Li, W. Tao, The influence of gaseous heat conduction to the effective thermal conductivity of nano-porous materials, *Int. Commun. Heat Mass Tran.* 68 (2015) 158–161.
- [19] G. Reichenauer, U. Heinemann, H.-Ebert, Relationship between pore size and the gas pressure dependence of the gaseous thermal conductivity, *Colloids Surf. A Physicochem. Eng. Asp.* 300 (1) (2007) 204–210.
- [20] J. Fricke, X. Lu, P. Wang, D. Büttner, U. Heinemann, Optimization of monolithic silica aerogel insulants, *Int. J. Heat Mass Tran.* 35 (9) (1992) 2305–2309.
- [21] M.G. Kaganer, A. Moscona, Thermal Insulation in Cryogenic Engineering, 1969.
- [22] X. Lu, M.C. Arduini-Schuster, J. Kuhn, O. Nilsson, J. Fricke, R.W. Pekala, Thermal conductivity of monolithic organic aerogels, *Science* 255 (5047) (1992) 971–972.
- [23] C. Bi, G.H. Tang, W.Q. Tao, Prediction of the gaseous thermal conductivity in aerogels with non-uniform pore-size distribution, *J. Non-Cryst. Solids* 358 (23) (2012) 3124–3128.
- [24] T. Xie, Y. He, Z. Hu, Theoretical study on thermal conductivities of silica aerogel composite insulating material, *Int. J. Heat Mass Tran.* 58 (1–2) (2013) 540–552.
- [25] F. Matter, A.L. Luna, M. Niederberger, From colloidal dispersions to aerogels: how to master nanoparticle gelation, *Nano Today* 30 (2020), 100827.
- [26] C. Zhu, Z. Li, H. Pang, N. Pan, Numerical modeling of the gas-contributed thermal conductivity of aerogels, *Int. J. Heat Mass Tran.* 131 (2019) 217–225.
- [27] B. Wang, L. Zhou, S.C. Lee, A fractal model for predicting the effective thermal conductivity of liquid with suspension of nanoparticles, *Int. J. Heat Mass Tran.* 46 (14) (2003) 2665–2672.
- [28] J. Zhao, Y. Duan, X. Wang, B. Wang, A 3-D numerical heat transfer model for silica aerogels based on the porous secondary nanoparticle aggregate structure, *J. Non-Cryst. Solids* 358 (10) (2012) 1287–1297.
- [29] G. Lu, X. Wang, Y. Duan, X. Li, Effects of non-ideal structures and high temperatures on the insulation properties of aerogel-based composite materials, *J. Non-Cryst. Solids* 357 (22) (2011) 3822–3829.
- [30] W.H. McCrea, *Theoretical Astrophysics. Atomic theory and the analysis of stellar atmospheres and envelopes*, 355. 25s, in: S. Rosseland, Pp xix (Eds.), *International series of monographs on physics*. (Oxford). *Mathematical gazette* 20 (241) (1936) 342–344, 1936.
- [31] G. Mie, Beiträge zur Optik trüber Medien, speziell kolloidaler Metallösungen, *Ann. Phys.* 330 (3) (1908) 377–445.
- [32] R.R. Cunningham, S.C. Lee, Radiative properties of fibrous insulations: theory versus experiment, *J. Thermophys. Heat Tran.* 10 (3) (1996) 460–466.
- [33] Y. He, T. Xie, Advances of thermal conductivity models of nanoscale silica aerogel insulation material, *Appl. Therm. Eng.* 81 (2015) 28–50.
- [34] C.L. Tien, G. Chen, Challenges in microscale conductive and radiative heat transfer, *J. Heat Tran.* 116 (4) (1994) 799–807.
- [35] D.G. Cahill, P.V. Braun, G. Chen, D.R. Clarke, S. Fan, K.E. Goodson, P. Keblinski, W.P. King, G.D. Mahan, A. Majumdar, H.J. Maris, S.R. Phillpot, E. Pop, L. Shi, Nanoscale thermal transport. II. 2003–2012, *Appl. Phys. Rev.* 1 (1) (2014), 11305.
- [36] S. Vivod, M. Meador, L. Capadona, R. Sullivan, L. Ghosn, N. Clark, L. McCorkle, D. Quade, Carbon nanofiber incorporated silica based aerogels with di-isocyanate cross-linking, *American Chemical Society, Polymer Preprints, Division of Polymer Chemistry* 49 (2008) 306–307.
- [37] J. Cai, S. Liu, J. Feng, S. Kimura, M. Wada, S. Kuga, L. Zhang, Cellulose-silica nanocomposite aerogels by in-situ formation of silica in cellulose gel, *Angew. Chem.* 51 (9) (2012) 2076–2079.
- [38] L. Tong, J. Lou, R.R. Gattass, S. He, X. Chen, L. Liu, E. Mazur, Assembly of silica nanowires on silica aerogels for microphotonic devices, *Nano Lett.* 5 (2) (2005) 259.
- [39] S.P. Patil, P. Shendye, B. Markert, Molecular dynamics simulations of silica aerogel nanocomposites reinforced by glass fibers, graphene sheets and carbon nanotubes: a comparison study on mechanical properties, *Compos. B Eng.* 190 (2020), 107884.
- [40] O.A. Madyan, M. Fan, Temperature induced nature and behaviour of clay-PVA colloidal suspension and its aerogel composites, *Colloids Surf. A Physicochem. Eng. Asp.* 529 (2017) 495–502.

- [41] O.A. Madyan, M. Fan, Hydrophobic clay aerogel composites through the implantation of environmentally friendly water-repellent agents, *Macromolecules* 51 (24) (2018) 10113–10120.
- [42] O.A. Madyan, M. Fan, Organic functionalization of clay aerogel and its composites through in-situ crosslinking, *Appl. Clay Sci.* 168 (2019) 374–381.
- [43] O.A. Madyan, M. Fan, Z. Huang, Functional clay aerogel composites through hydrophobic modification and architecture of layered clays, *Appl. Clay Sci.* 141 (2017) 64–71.
- [44] O.A. Madyan, M. Fan, L. Feo, D. Hui, Enhancing mechanical properties of clay aerogel composites: an overview, *Compos. B Eng.* 98 (2016) 314–329.
- [45] O.A. Madyan, M. Fan, L. Feo, D. Hui, Physical properties of clay aerogel composites: an overview, *Compos. B Eng.* 102 (2016) 29–37.
- [46] M. Cao, B. Liu, L. Zhang, Z. Peng, Y. Zhang, H. Wang, H. Zhao, Y. Wang, Fully biomass-based aerogels with ultrahigh mechanical modulus, enhanced flame retardancy, and great thermal insulation applications, *Compos. B Eng.* 225 (2021), 109309.
- [47] T. Xue, W. Fan, X. Zhang, X. Zhao, F. Yang, T. Liu, Layered double hydroxide/graphene oxide synergistically enhanced polyimide aerogels for thermal insulation and fire-retardancy, *Compos. B Eng.* 219 (2021), 108963.
- [48] J. Zhu, F. Zhao, T. Peng, H. Liu, L. Xie, C. Jiang, Highly elastic and robust hydroxyapatite nanowires/polyimide composite aerogel with anisotropic structure for thermal insulation, *Compos. B Eng.* 223 (2021), 109081.
- [49] J. Sun, Z. Wu, B. An, C. Ma, L. Xu, Z. Zhang, S. Luo, W. Li, S. Liu, Thermal-insulating, flame-retardant and mechanically resistant aerogel based on bio-inspired tubular cellulose, *Compos. B Eng.* 220 (2021), 108997.
- [50] R.H. Nosrati, U. Berardi, Hygrothermal characteristics of aerogel-enhanced insulating materials under different humidity and temperature conditions, *Energy Build.* 158 (2018) 698–711.
- [51] U. Berardi, R.H. Nosrati, Long-term thermal conductivity of aerogel-enhanced insulating materials under different laboratory aging conditions, *Energy* 147 (2018) 1188–1202.
- [52] X. Ye, Z. Chen, S. Ai, B. Hou, J. Zhang, Q. Zhou, F. Wang, H. Liu, S. Cui, Microstructure characterization and thermal performance of reticulated SiC skeleton reinforced silica aerogel composites, *Compos. B Eng.* 177 (2019), 107409.
- [53] S. Liu, V.S. Chevali, Z. Xu, D. Hui, H. Wang, A review of extending performance of epoxy resins using carbon nanomaterials, *Compos. B Eng.* 136 (2018) 197–214.
- [54] A.L. Loeb, Thermal conductivity: VIII, A theory of thermal conductivity of porous materials, *J. Am. Ceram. Soc.* 37 (2) (1954) 96–99.
- [55] S.S. Kistler, The Relation between heat conductivity and structure in silica aerogel, *J. Phys. Chem.* 39 (1) (1935) 79–86.
- [56] S.Q. Zeng, A. Hunt, R. Greif, Mean free path and apparent thermal conductivity of a gas in a porous medium, *J. Heat Tran.* 117 (3) (1995) 758–761.
- [57] F. Hemberger, S. Weis, G. Reichenauer, H. Ebert, Thermal transport properties of functionally graded carbon aerogels, *Int. J. Thermophys.* 30 (4) (2009) 1357–1371.
- [58] S.Q. Zeng, A. Hunt, R. Greif, Transport properties of gas in silica aerogel, *J. Non-Cryst. Solids* 186 (1995) 264–270.
- [59] J. Wang, J. Kuhn, X. Lu, Monolithic silica aerogel insulation doped with TiO₂ powder and ceramic fibers, *J. Non-Cryst. Solids* 186 (1995) 296–300.
- [60] S. Lee, G. Cunningham, Conduction and radiation heat transfer in high-porosity fiber thermal insulation, *J. Thermophys. Heat Tran.* 14 (2000) 121–136.
- [61] C. Bi, G.H. Tang, Z.J. Hu, Heat conduction modeling in 3-D ordered structures for prediction of aerogel thermal conductivity, *Int. J. Heat Mass Tran.* 73 (2014) 103–109.
- [62] S.Q. Zeng, A. Hunt, R. Greif, Geometric structure and thermal conductivity of porous medium silica aerogel, *J. Heat Tran.* 117 (4) (1995) 1055–1058.
- [63] J. Zhao, Y. Duan, X. Wang, B. Wang, Effects of solid–gas coupling and pore and particle microstructures on the effective gaseous thermal conductivity in aerogels, *J. Nanoparticle Res.: An Interdisciplinary Forum for Nanoscale Science and Technology* 14 (8) (2012) 1–15.
- [64] L. Masanes, J. Oppenheim, A general derivation and quantification of the third law of thermodynamics, *Nat. Commun.* 8 (1) (2017), 14538.
- [65] J. Feng, M. Liu, S. Ma, J. Yang, W. Mo, X. Su, Micro-nano scale heat transfer mechanisms for fumed silica based thermal insulating composite, *Int. Commun. Heat Mass Tran.* 110 (2020), 104392.
- [66] R.L. Hamilton, O.K. Crosser, Thermal conductivity of heterogeneous two-component systems, *Ind. Eng. Chem. Fundam.* 1 (3) (1962) 187–191.
- [67] J. Zhao, Y. Duan, X. Wang, B. Wang, An analytical model for combined radiative and conductive heat transfer in fiber-loaded silica aerogels, *J. Non-Cryst. Solids* 358 (10) (2012) 1303–1312.
- [68] J.C.M. Garnett, Colours in metal glasses and in metallic films, *Proc. Roy. Soc. Lond.* 73 (488) (1904) 443–445.
- [69] G. Wei, X. Zhang, F. Yu, Effective thermal conductivity analysis of xonotlite-aerogel composite insulation material, *J. Therm. Sci.* 18 (2) (2009) 142–149.
- [70] D. Dan, H. Zhang, W. Tao, Effective structure of aerogels and decomposed contributions of its thermal conductivity, *Appl. Therm. Eng.* 72 (1) (2014) 2–9.
- [71] P. Cheng, C. Hsu, The effective stagnant thermal conductivity of porous media with periodic structures, *J. Porous Media* 2 (1) (1999) 19–38.
- [72] S. Spagnol, B. Lartigue, A. Trombe, V. Gibiat, Thermal modelling of two-dimensional periodic fractal patterns, an application to nanoporous media, *Europhys. Lett.* 78 (4) (2007), 46005.
- [73] P. Meakin, R. Jullien, The effects of restructuring on the geometry of clusters formed by diffusion-limited, ballistic, and reaction-limited cluster-cluster aggregation, *J. Chem. Phys.* 89 (1) (1988) 246–250.
- [74] J. Primera, A. Hasmy, T. Woignier, Numerical study of pore sizes distribution in gels, *J. Sol. Gel Sci. Technol.* 26 (1) (2003) 671–675.
- [75] M. Wang, N. Pan, Predictions of effective physical properties of complex multiphase materials, *Mater. Sci. Eng. R Rep. : a review journal* 63 (1) (2008) 1–30.
- [76] S.Q. Zeng, A. Hunt, R. Greif, Theoretical modelling of carbon content to minimize heat transfer in silica aerogel, *J. Non-Cryst. Solids* 186 (1995) 271–277.
- [77] Debye PP. *Light Scattering by Small Particles*. H. C. Van de Hulst. Wiley, New York; Chapman & Hall, London, 1957. xiii+470 pp. Illus. \$12. Science (American Association for the Advancement of Science) 1958;vol. 127(3296):477-478.
- [78] S.Q. Zeng, A.J. Hunt, R. Grief, W. Cao, Approximate formulation for coupled conduction and radiation through a medium with arbitrary optical thickness, *J. Heat Tran.* 117 (3) (1995) 797–799.
- [79] H. Liu, X. Xia, X. Xie, Q. Ai, D. Li, Experiment and identification of thermal conductivity and extinction coefficient of silica aerogel composite, *Int. J. Therm. Sci.* 121 (2017) 192–203.